

Title

Epigenetic Memory Independent of Symmetric Histone Inheritance

Authors

Daniel S Saxton¹, Jasper Rine¹

¹Department of Molecular and Cell Biology, University of California, Berkeley, Berkeley, United States

Abstract

Heterochromatic gene silencing is an important form of gene regulation that usually requires specific histone modifications. A popular model posits that inheritance of modified histones, especially in the form of H3-H4 tetramers, underlies inheritance of heterochromatin. Because H3-H4 tetramers are randomly distributed between daughter chromatids during DNA replication, rare occurrences of asymmetric tetramer inheritance within a heterochromatic domain would have the potential to destabilize heterochromatin. This model makes a prediction that shorter heterochromatic domains would experience unbalanced tetramer inheritance more frequently, and thereby be less stable. In contrast to this prediction, we found that shortening a heterochromatic domain in *Saccharomyces* had no impact on the strength of silencing nor its heritability. Additionally, we found that replisome mutations that disrupt inheritance of H3-H4 tetramers had only minor effects on heterochromatin stability. These findings suggest that histones carry little or no memory of the heterochromatin state through DNA replication.

23

24 **Introduction**

25 A central question in biology is how cells with identical genotypes can exhibit different,
26 heritable phenotypes. By definition, these phenotypes are determined by information that is
27 epigenetic, or “above the genome.” Just as genetic inheritance requires faithful replication of
28 DNA, epigenetic inheritance requires replication of information that is transmitted to both
29 daughter cells during division. Faithful transmission of epigenetic information is crucial for
30 multiple heterochromatin-based processes such as X-chromosome inactivation in mammals
31 and cold-induced gene silencing in *Arabidopsis*. In these cases and others, the epigenetic
32 inheritance of heterochromatin indicates that some components of heterochromatin must
33 behave as heritable units. Surprisingly, the identity of this epigenetic information remains
34 unclear and heavily debated.

35 The histone subunits of nucleosomes, especially histones H₃ and H₄, are modified by a
36 variety of covalent modifications that are integral to heterochromatin function. During DNA
37 replication, nucleosomes are partially disrupted and marked parental H₃-H₄ tetramers are
38 locally inherited to daughter chromatids. As these tetramers are inherited, they are
39 reassembled into nucleosomes that are interspersed with nucleosomes containing newly
40 synthesized H₃-H₄ tetramers (Prior et al. 1980; Jackson 1988; Schlissel & Rine 2019). One
41 model for epigenetic inheritance posits that marked parental histones inherited through DNA
42 replication recruit histone modifiers to deposit similar marks on new adjacent nucleosomes,
43 thereby reestablishing the previous local landscape of histone modifications (Hecht et al. 1995;
44 Hoppe et al. 2002; Gaydos et al. 2014). In support of this model, the H₃K27 methyltransferase

PRC2 binds preferentially to H3K27me₃ *in vitro* (Hansen et al. 2008) and some other modifying enzymes show a similar ability to bind their histone modifications (Zhang et al. 2008; Hecht et al. 1995; Imai et al. 2000). If this model is correct, modified H₃-H₄ tetramers would constitute heritable units that drive epigenetic memory of chromatin states.

Studies have come to different conclusions regarding whether histones can carry epigenetic memory. In *S. pombe*, localized methylation of H3K9 can silence a reporter gene, and this silenced state is heritable in the presence of the H3K9 methyltransferase Clr4p as long as the demethylase Epe1p is absent (Audergon et al. 2015; Ragunathan et al. 2015). These studies suggest that histone modifications can facilitate epigenetic inheritance, and caution that such a mechanism is normally obscured by H3K9 demethylation activity. Conversely, induced removal of silencer elements from silenced chromatin in *S. cerevisiae* causes almost all cells to lose silencing of adjacent genes after just one round of DNA replication (Holmes & Broach 1996). Similar results are found when silencers are removed from *Drosophila* chromatin silenced by the Polycomb complex (Laprell et al. 2017). These silencer-removal experiments suggest that modified histones are not sufficient to propagate the silenced chromatin state through DNA replication.

The model in which histones carry epigenetic memory makes a testable prediction: since parental H₃-H₄ tetramers have long been thought to be randomly partitioned between daughter chromatids (Sogo et al. 1986; Cusick et al. 1984), rare events could occur in which most or all marked parental H₃-H₄ tetramers within a domain segregate asymmetrically to one daughter chromatid, causing the other to inherit primarily newly synthesized histones. A chromatin domain with an insufficient number of marked parental tetramers would be

67 expected to experience a loss-of-chromatin-state event. In this view, a smaller chromatin
68 domain would correspond to fewer marked nucleosomes and yield more frequent events in
69 which parental H₃-H₄ tetramers segregate asymmetrically and the chromatin state is lost. This
70 potential use of domain size for protection against epimutation is widely conjectured (Dodd et
71 al. 2007; Kaufman & Rando 2010; Moazed 2011; Ramachandran & Henikoff 2015), and may
72 explain why chromatin domains subject to stable epigenetic inheritance are often many
73 kilobases long. For example, chromatin domains silenced by Polycomb Responsive Elements
74 (PREs) in *Drosophila* usually extend beyond 10 kb (Schwartz et al. 2006). In contrast, one study
75 in *A. thaliana* found that a chromatin domain containing only three H₃K₂₇me₃-marked
76 nucleosomes is inherited more frequently than would be predicted if random segregation of
77 tetramers caused loss events (Yang et al. 2017). However, no study to our knowledge has
78 systematically tested this prediction.

79 To test directly whether inheritance of a chromatin state is affected by chromatin-
80 domain size, we focused on the heterochromatin domains at the *HMR* and *HML* loci in *S.*
81 *cerevisiae*. These loci contain copies of mating-type genes that are silenced by the activity of
82 Sir proteins. Specifically, the *E* and *I* silencers flanking *HMR* and *HML* are occupied by the DNA-
83 binding proteins Rap1, Abf1, and ORC, that collectively recruit Sir proteins; Sir1 is present only
84 at silencers, whereas Sir2/3/4 complexes bind to silencers and spread across the locus in a
85 process that requires deacetylation of H₄K16 (Rusché et al. 2002; Thurtle & Rine 2014).
86 Notably, DNA methylation and RNA interference do not exist in *S. cerevisiae*.

87 Under normal conditions, *HMR* and *HML* are constitutively silenced. Rare and transient
88 loss-of-silencing events can be measured by a sensitive assay that uses the *cre* recombinase

under control of the *HML* α 2 promoter to convert transient transcriptional events into permanent, heritable changes in fluorescence phenotypes (Dodson & Rine 2015). In contrast, deletion of *SIR1* causes genetically identical cells to be in either of two states at *HMR* and *HML*: either fully silenced or fully expressed (Pillus & Rine 1989; E. Y. Xu et al. 2006; Dodson & Rine 2015). These different transcriptional states are mitotically heritable and cells switch between states at a low frequency. This study addresses three questions regarding the inheritance of heterochromatin in *Saccharomyces*: 1) Does the size of a silenced domain determine the fidelity of inheritance? 2) Does removal of Sir1, a protein that facilitates recruitment of silencing machinery to silencers, uncover an effect of chromatin domain size on heritability of transcriptional states? 3) Do replisome components that facilitate symmetric inheritance of parental H3-H4 tetramers also promote inheritance of transcriptional states?

Results

Local inheritance of nucleosomes and their locus-specific modifications are thought to facilitate inheritance of chromatin states. According to this view, if parental H3-H4 tetramers were randomly partitioned between the two daughter chromatids during replication, one would expect a chromatin state to be lost if, by chance, one of the daughter chromatids failed to receive enough parental H3-H4 tetramers to support the propagation of that state. By this model, the number of nucleosomes in the chromatin domain would influence the fidelity of chromatin-state inheritance.

Nucleosome number did not determine the rate of silencing loss

To test if nucleosome number affected the stable inheritance of a chromatin state, we used the Cre-Reported Altered States of Heterochromatin (CRASH) assay (Dodson & Rine 2015) (Figure 1A). In this assay, *cre* replaces the $\alpha 2$ coding sequence in *HMR α* , and a *lox* cassette containing fluorescent reporters separated by *loxP* sites is located on a separate chromosome. Though *HMR α* is transcriptionally repressed, rare loss-of-silencing events cause transient expression of *cre*. These events lead to excision of *RFP* from the *lox* cassette, and a switch from RFP to GFP expression. Because this change is heritable, loss-of-silencing events during colony growth lead to formation of sectors of cells expressing GFP, appearing green on an otherwise red background. The number of sectors in a colony reflects the frequency at which *HMR α* transiently loses silencing: more sectors indicate less stable silencing.

HMR α ::cre contained fourteen well-positioned nucleosomes between the *E* and *I* silencers (Figure 1-figure supplement 1). To change nucleosome number within the locus, we deleted DNA corresponding to different sets of nucleosomes (Figure 1B). Notably, removing DNA corresponding to different combinations of well-positioned nucleosomes allowed us to discern whether any effects on silencing stability were due to nucleosome number or to removal of specific DNA sequences. These deletions did not affect the local positions of the remaining nucleosomes as measured by MNase-Seq (Figure 1-figure supplement 1).

At the limit of models by which nucleosomes transmit memory of transcriptional states, inheritance of a single parental H₃-H₄ tetramer to a daughter chromatid would be sufficient to template the silenced state. The expected loss-of-silencing rate would thereby reflect the frequency at which a chromatid inherits no marked parental H₃-H₄ tetramers due to random segregation of these tetramers during replication. For example, considering a

hypothetical chromatin domain that has three nucleosomes, one would expect that a given daughter chromatid would have a one-in-eight chance of inheriting no parental tetramers during replication. Therefore, one in eight daughter cells would be expected to lose silencing. This rate would increase exponentially with shorter chromatin domains as the probability of inheriting at least one parental tetramer decreases (Figure 1C). Additionally, if inheritance of two or more parental H₃-H₄ tetramers was necessary to template the silenced state, the expected loss-of-silencing rate would be even higher.

The silencing-loss rate predicted by random segregation of H₃-H₄ tetramers would be approximately 0.006% of cell divisions for full-length *HMR α ::cre* (Strain N14) (Figure 1D). Previous studies demonstrate that this strain loses silencing in approximately 0.1% of cell divisions (Dodson & Rine 2015). This difference between expected and observed values could be explained by the existence of other processes besides histone inheritance that potentially destabilize silencing and thereby contribute to the overall silencing-loss rate. In contrast to the full size *HMR α ::cre*, the smallest version of *HMR α ::cre* (Strain N7) would be expected to lose silencing in approximately 1% of cell divisions (Figure 1D). Therefore, if this model were correct, we would expect to see increased sectoring rates in strains with shorter versions of *HMR α ::cre*. Surprisingly, decreasing nucleosome number at *HMR α ::cre* led to a slight decrease in silencing loss as measured by sector frequency (Figure 1E).

To provide an independent measurement of the silencing-loss rate, we also measured fluorescence profiles of single cells. Cells that have recently lost silencing of *cre* at *HMR α* contain both RFP and GFP due to GFP expression and the persistence of RFP prior to its degradation and dilution. Using flow cytometry to measure the frequency of cells that contain

155 both RFP and GFP, we confirmed that nucleosome number did not strongly affect silencing-
156 loss rates, and that reduction of nucleosomes might have a slight stabilizing effect on silencing
157 (Figure 1F, Figure 1-figure supplement 2). Thus, the size of *HMR α ::cre* did not dramatically
158 influence inheritance of the silenced state, in contrast to the expectation from models in which
159 H3-H4 tetramers carry memory of chromatin states through cell divisions. Additionally, we
160 found that changing nucleosome number at *HML α ::cre* led to a small increase in silencing loss,
161 and that these effects were not due strictly to domain size (Figure 1-figure supplements 3-5).
162 Since studies at *HML α* are potentially complicated by its proximity to a telomere, which is also
163 bound by Sir proteins, further studies were performed only at *HMR α* .

Nucleosome number did not affect transmission of epigenetic states in *sir1Δ*.

The silencers flanking *HMRα* are bound by three different proteins that collaborate to recruit Sir proteins (Rusché et al. 2003). One possibility for the apparent insensitivity of silencing inheritance to nucleosome number was that the constant recruitment of Sir proteins to these sites was efficient enough to mask a contribution of histone inheritance to inheritance of chromatin states. In this scenario, silencers would be capable of recruiting enough Sir proteins to keep the locus silenced during DNA replication, regardless of histone segregation patterns. Sir1 binds to silencers, and deletion of *SIR1* partially disrupts silencer activity, as measured by defects in silencing establishment and silencing heritability (Pillus & Rine 1989; Dodson & Rine 2015). We therefore tested if parental H3-H4 tetramer inheritance contributed to transmission of the silenced state when silencer-based recruitment of Sir proteins was impaired by the *sir1Δ* mutation.

Within individual cells in a population of *sir1Δ* cells, *HMR* is either transcriptionally silenced or fully expressed. These different states are mitotically heritable: a cell in one state usually gives rise to more cells of that state. To observe this epigenetic phenomenon, we placed the *GFP* coding sequence into *HMRα*, such that it was expressed under control of the $\alpha 2$ promoter. Silencing was monitored by GFP expression at the single-cell level using fluorescence microscopy and flow cytometry. In comparison to control strains in which *HMRα* was fully silenced (*SIR+*) or expressed (*sir4Δ*), *HMRα* was silenced in roughly 99% of *sir1Δ* cells and was expressed in the remaining cells (Figure 2-figure supplement 1,2). We also observed different epigenetic states for *HMLα::RFP*. We used live-cell imaging to monitor divisions of

sir1Δ cells to identify cells in which silencing of *HMR* was lost, and other cases in which it was gained (Figure 2A, Video 1). Thus *HMRα::GFP* could be used to measure the efficiency of epigenetic inheritance in *sir1Δ*, similarly to previous studies (E. Y. Xu et al. 2006). For simplicity, we named measurements of epigenetic inheritance in *sir1Δ* as the FLuorescent Analysis of Metastable Expression (FLAME) assay, which is commonly implemented by live cell microscopy but is also adapted to flow cytometry as noted in individual experiments.

To test the prediction that chromatin domain size affects silencing heritability with the FLAME assay, we removed DNA corresponding to sets of nucleosomes in the *HMRα::GFP* locus (Figure 2B, Figure 2-figure supplement 3,4). As before, models in which nucleosomes were carriers of epigenetic memory predicted that shorter chromatin domains would have a higher rate of silencing loss (Figure 2C). Using time-lapse fluorescence microscopy to monitor transcriptional states in individual cells and their descendants as they divided, we found that nucleosome number did not affect the frequency of silencing loss (Figure 2D). Because the expressed state is also heritable, with occasional switches to the silenced state, we also asked if the heritability of the expressed state was influenced by the number of nucleosomes in the locus. The frequency of silencing establishment was similar between strains with different numbers of nucleosomes at *HMRα::GFP* (Figure 2E). Therefore, even in a background with defective silencer activity, chromatin-domain size did not strongly influence silencing dynamics. These findings argued against models in which parental H₃-H₄ tetramers and their modifications are required for the epigenetic inheritance of gene expression states in *Saccharomyces*.

Replisome defects affected epigenetic inheritance

An orthogonal approach to test the role of histones in carrying epigenetic memory would be to consistently bias parental H₃-H₄ tetramer inheritance to one daughter chromatid, leaving the other daughter chromatid with fewer parental H₃-H₄ tetramers. Recent reports demonstrate conserved roles of two replisome components, Dpb3 and Mcm2, in producing a more symmetric distribution of parental H₃-H₄ tetramers between the leading and lagging strands. Specifically, *dpb3Δ* causes biased parental H₃-H₄ tetramer inheritance to the lagging strand (Yu et al. 2018) and a set of point mutations in *MCM2* (*mcm2-3A*) causes biased parental H₃-H₄ tetramer inheritance to the leading strand (Petryk et al. 2018; Gan et al. 2018). A complementary study that was able to observe local inheritance of histone H₄ in a small chromatin domain, though was unable to distinguish leading versus lagging strand biases, found that local histone H₄ inheritance was moderately reduced in both the *dpb3Δ* and *mcm2-3A* single mutants, and severely reduced in the *dpb3Δ mcm2-3A* double mutant (Schlissel & Rine 2019). Together, these studies demonstrate that Dpb3 and Mcm2 are necessary for efficient inheritance of parental H₃-H₄ tetramers to both daughter chromatids during DNA replication.

If parental H₃-H₄ tetramer inheritance contributes to transmission of chromatin states, we would predict more loss-of-silencing events in strains with defects in tetramer inheritance. To test this idea, we measured silencing loss in replisome mutants using the CRASH assay (Figure 3A). The *dpb3Δ* and *mcm2-3A* single mutants exhibited higher silencing-loss rates, consistent with previous studies done at *HML* (Yu et al. 2018; Gan et al. 2018), and the *dpb3Δ mcm2-3A* double mutant lost silencing more frequently than either single mutant. Similar

results were obtained by using flow cytometry to measure silencing-loss rates (Figure 3B). These data were consistent with a model in which inheritance of parental H₃-H₄ tetramers could contribute to inheritance of the silenced state at *HMR*. However, the data were also compatible with the possibility that heterochromatin assembled in such mutants was simply unstable for reasons independent of defects in its inheritance. Additionally, since previous studies did not specifically test the effects of Dpb3 and Mcm2 on histone inheritance within heterochromatin, any interpretations of silencing defects operated under the assumption that these replisome components act similarly between heterochromatin and euchromatin.

It is possible that parental H₃-H₄ tetramer inheritance affects both transient loss-of-silencing events, as detected by the CRASH assay, and heritability of epigenetic states. Testing this possibility was important because the currently unidentified epigenetic information that determines expression states in *sir1Δ* is transmitted locally at *HML* and *HMR*, respectively, rather than being transmitted in *trans* from processes elsewhere in the cell (E. Y. Xu et al. 2006). If parental H₃-H₄ tetramers were the crucial local factors that transmitted this information, we would predict that disrupted tetramer inheritance would cause more loss-of-silencing events in *sir1Δ*. To test this possibility, we generated replisome mutant strains in combination with *sir1Δ* and evaluated the inheritance of transcriptional states using two different FLAME assay measurements: Fluorescence-Activated Cell Sorting (FACS) and live-cell microscopy.

Populations of *dpb3Δ*, *mcm2-3A*, and *dpb3Δ mcm2-3A* mutants all showed a mix of cells that were silenced or expressed at *HMRα::GFP*; all three mutant strains also showed a higher frequency of expressed cells than wildtype (Figure 4-figure supplement 1, Table 1). Because

silencing-loss rates and silencing-establishment rates both affect the frequency of cells in which *HMR* is silenced or expressed, one or both of these rates were presumably different in replisome mutants. To measure these rates, we used FACS to sort cells from each strain into two separate populations of *HMR*-silenced and *HMR*-expressed cells, and used flow cytometry to monitor the rates at which these initial sorted populations relaxed back to a mixed population of silenced and expressed cells (Figure 4A). These relaxation rates, and the frequency of silenced cells at equilibrium, were a product of competing silencing-loss and silencing-establishment rates. By using these relaxation rates to calculate silencing-loss rates (Figure 4B, Figure 4-figure supplement 2), we observed that *dpb3Δ* and *mcm2-3A* had a higher loss-of-silencing rate than wildtype (Figure 4C). The *dpb3Δ mcm2-3A* double mutant had a higher loss rate than the single mutants. Similar loss trends were observed using time-lapse fluorescence microscopy (Figure 4D), albeit with overall higher loss rates than those seen with FACS sorting. Together, these data suggested that faithful inheritance of parental H₃-H₄ tetramers helped transmit the silenced state of *HMR*. However, we also noted that the vast majority of silenced cells still faithfully transmitted the silenced state in the replisome mutant backgrounds.

We also asked if replisome mutants had differences in the frequency of silencing-establishment events. Curiously, any strain containing *dpb3Δ* had an increased establishment rate, whereas *mcm2-3A* had minimal, if any, effects on establishment rate (Figure 4E-G). Additionally, any strain containing *dpb3Δ* showed elevated levels of *HMRα::GFP* expression in unsilenced cells, as measured by flow cytometry (Figure 4-figure supplement 3). Because *dpb3Δ* cells more readily established silencing, we inferred that the expressed state was less

efficiently inherited. Therefore, Dpb3 contributed to the inheritance of the expressed state of *HMR* as well as to the silenced state.

Variations in nucleosome number in replisome mutant backgrounds

Though the rate of silencing loss increased in replisome mutant backgrounds, the large majority of silenced cells still faithfully transmitted the silenced state through cell divisions. Indeed, though *dpb3Δ* and *mcm2-3A* single mutants exhibit asymmetric parental H₃-H₄ tetramer inheritance (Yu et al. 2018; Petryk et al. 2018), it is likely that this asymmetry is not complete and some parental H₃-H₄ tetramers are still stochastically transmitted to each daughter chromatid during DNA replication. Similarly, the *dpb3Δ mcm2-3A* double mutant exhibits residual local inheritance of histone H₄ (Schlissel & Rine 2019). We reasoned that, if a daughter chromatid consistently inherits fewer parental H₃-H₄ tetramers and thereby loses the silenced state more frequently, an additional reduction in the size of a chromatin domain would cause that daughter chromatid to inherit even fewer marked parental H₃-H₄ tetramers and experience loss-of-silencing events even more frequently. Therefore, if parental H₃-H₄ tetramers carry epigenetic memory, we would expect loci with fewer nucleosomes to exhibit more loss-of-silencing events in replisome mutant backgrounds. To test his idea, we used the FLAME assay on nucleosome-number mutants in *dpb3Δ* and *dpb3Δ mcm2-3A* strains (Figure 5A, figure 5-figure supplement 1). There was no clear correlation between silencing-loss rates and nucleosome number in these sensitized backgrounds (Figure 5B). Establishment-of-silencing rates were also not strongly affected, though there was a small increase in the establishment rate with fewer nucleosomes in *dpb3Δ mcm2-3A* (Figure 5C). Therefore, even

when parental H₃-H₄ tetramer inheritance was disrupted and the number of parental H₃-H₄ tetramers available for inheritance at *HMR* was decreased, cells faithfully transmitted epigenetic transcriptional states.

Discussion

Heterochromatin is frequently characterized by specific histone modifications bound by silencing proteins; these components are critical to mechanisms of silencing and have long been considered as mediators of epigenetic inheritance. A popular model is that modified H₃-H₄ tetramers are heritable units of epigenetic information that are randomly segregated between daughter chromatids during DNA replication (Ramachandran & Henikoff 2015). Models founded on random segregation of parental H₃-H₄ tetramers predict that shorter chromatin domains would decrease the heritability of chromatin states in those domains. Contrary to the prediction, we found that shortening the silenced chromatin domain at *HMR* had no significant effects on silencing-loss rate as measured by the CRASH and FLAME assays, even in mutants lacking a component of the silencer-binding complex and in mutants with defective versions of two different regulators of parental H₃-H₄ tetramer segregation.

Evidence that H₃-H₄ Tetramers Did Not Carry Epigenetic Memory

Removal of silencers from heterochromatin via induced recombination demonstrates that silencers are necessary for maintenance of the silenced state. Specifically, induced silencer excision from *HMR* causes rapid loss of silencing in arrested cells (Cheng & Gartenberg 2000). Studies at other loci in *S. cerevisiae* and *Drosophila* show that removal of silencers permits

318 maintenance of silencing in arrested cells, but causes loss of silencing once the same cells
319 subsequently complete one or two rounds of DNA replication (Holmes & Broach 1996; Laprell
320 et al. 2017). Therefore, the presence of modified histones is not sufficient for silencing
321 maintenance or heritability, depending on the example under consideration. Indeed, given that
322 silencers are constantly recruiting Sir proteins to these loci, any role of H₃-H₄ tetramers in
323 transmission of epigenetic information might be hard to detect.

324 We considered the possibility that silencer activity masks an underlying contribution of
325 H₃-H₄ tetramer inheritance to silencing inheritance. However, the weakened silencer activity
326 in *sir1Δ* mutants did not reveal a sensitivity of silencing inheritance to the size of the silenced
327 domain at *HMR*. Importantly, epigenetic states of *HML* and *HMR* in *sir1Δ* are a property of the
328 locus rather than the cell, demonstrating that factors that determine these epigenetic states
329 are inherited locally at *HML* and *HMR* respectively (E. Y. Xu et al. 2006). Similar studies of an
330 epigenetically-inherited heterochromatin state in *Arabidopsis* also demonstrate that the
331 relevant epigenetic information is carried in *cis* (Berry et al. 2015). Additionally, epigenetic
332 inheritance of transcriptional states in heterochromatin is commonly accompanied by the
333 ability to switch stochastically between states, a feature that implies the existence of
334 imperfectly heritable epigenetic information. Though modified H₃-H₄ tetramers could
335 theoretically be *cis*-acting, imperfectly heritable units of information, our evidence to the
336 contrary suggests that other *cis*-acting factors determine the epigenetic state of *HMR* in *sir1Δ*.
337 Given the importance of silencers in inheritance of the silenced chromatin state, one possibility
338 is that the silencer complex self-templates by cooperative oligomerization of silencing factors,

and that stochastic changes in epigenetic states reflect the formation or dissolution of such a silencer complex.

Addressing the Possibility that Tetramer Inheritance is Not Random

Classic studies of chromatin replication indicate that parental H₃-H₄ tetramers are randomly segregated between daughter chromatids during DNA replication. For example, chromatin replicated in the presence of cycloheximide, which blocks the synthesis of new histones, produces daughter chromatids with roughly half the number of nucleosomes, and these nucleosomes appear randomly dispersed along both daughter chromatids (Sogo et al. 1986; Cusick et al. 1984). Though our experiments built on these classic findings, it is also possible that parental H₃-H₄ tetramers may not be randomly segregated genome wide, or at *HMR* in particular. For example, it was possible that heterochromatin contained factors that facilitated alternating inheritance of tetramers between the leading and lagging strands. In this case, even if H₃-H₄ tetramers were to act as the sole units of epigenetic information, decreasing chromatin domain size might not affect the rate of silencing loss at *HMR*.

If H₃-H₄ tetramers carry epigenetic information through DNA replication, mutations that reduce tetramer inheritance would be expected to increase the frequency of silencing loss. Studies describe roles of Dpb3 and Mcm2 in heterochromatic silencing at *HML* (Yu et al. 2018; Gan et al. 2018), and inheritance of epigenetic states at a synthetic telomere (Iida & Araki 2003; Foltman et al. 2013). Using the CRASH and FLAME assays, we found mild but significant increases in *HMR* silencing-loss rates in both *dpb3Δ* and *mcm2-3A* single mutants. Additionally, the *dpb3Δ mcm2-3A* double mutant exhibited higher silencing-loss rates than either of the

single mutants. Together, these effects suggested that reduced tetramer inheritance caused mild defects in silencing heritability. Though deacetylated H₄K16 is crucial for silencing, other modifications such as H₃K56 acetylation also affect silencing (Hyland et al. 2005; F. Xu et al. 2007) and reduced inheritance of these modifications may hinder their functions. Considering the variety of histone modifications that parental H₃-H₄ tetramers can carry through DNA replication, it was striking that cells with moderate or severe reductions in inheritance of parental H₃-H₄ tetramers still exhibit robust inheritance of the silenced state.

Though replisome mutants exhibit defects in parental H₃-H₄ tetramer inheritance, some tetramers are still transmitted to both daughter chromatids in replisome mutant backgrounds (Yu et al. 2018; Gan et al. 2018; Schlissel & Rine 2019). Therefore, there are still parental tetramers that are theoretically capable of carrying epigenetic information to both daughter chromatids in the *dpb3Δ*, *mcm2-3A*, and *dpb3Δ mcm2-3A* mutants. Given that all replisome mutants tested showed increased silencing-loss rates, further reduction in the number of parental H₃-H₄ tetramers available for transmission to daughter chromatids should cause even higher rates of silencing loss. However, we saw no significant effects of *HMR* size on the silencing-loss rate in replisome mutant backgrounds. Therefore, cells with both reduced parental H₃-H₄ tetramer inheritance and a reduction in the number of tetramers available for inheritance at *HMR* exhibited a surprisingly robust ability to transmit the silenced state. These data strongly suggested that inheritance of parental H₃-H₄ tetramers has little or no impact on epigenetic inheritance of the silenced state of *HMR*.

Epigenetic Inheritance of the Expressed State

The expressed state of *HMR* in *sir1Δ* cells is formally an epigenetic state: it is heritable through cell divisions and can stochastically switch to the silenced state. One possibility is that the expressed state of *HMR* depends on the existence of heritable information, similarly to the silenced state. Histone modifications associated with active transcription can be transmitted through DNA replication (Alabert et al. 2015; Reverón-Gómez et al. 2018) and multiple transcription factors can bind to the histone modifications they generate (Jacobson et al. 2000; Owen et al. 2000). Therefore, histone modifications may form positive feedback loops with both silencing machinery and transcription factors. Indeed, a model that incorporates these positive feedback loops and parental H3-H4 tetramer inheritance generates robust bistable chromatin states (Dodd et al. 2007). This model also predicts that random segregation of parental H3-H4 tetramers would lead to loss-of-chromatin-state events, and that decreasing chromatin domain size would also decrease the heritability of both the expressed and silenced states. However, we found that shorter versions of *HMR* did not strongly affect inheritance of the expressed state of *HMR*.

Alternatively, if parental H3-H4 tetramers carry memory of the expressed state, mutations that disrupt parental H3-H4 tetramer inheritance would be expected to increase the rate of silencing establishment. Curiously, *dpb3Δ* exhibited a ~3-fold increase in the rate of silencing establishment and *mcm2-3A* had no observable effect. These data may suggest that parental tetramer inheritance facilitates heritability of the expressed state, though such an explanation could not account for the *mcm2-3A* phenotype. Alternatively, these data may suggest that inheritance of the expressed state is influenced by a function of Dpb3p that is separate from its role in tetramer inheritance. It is also important to note that *dpb3Δ* but not

405 *mcm2-3A* led to elevated levels of GFP expression when *HMRα::GFP* was fully expressed. This
406 finding is paradoxical, as one would expect elevated transcription to inhibit silencing
407 establishment, rather than facilitate it. However, recruitment of the transcriptional activator
408 Ppr1 to *HMR* causes both increased transcription in expressed cells and an increased
409 establishment rate in *sir1Δ* (E. Y. Xu et al. 2006).

410 Together, our results suggested that the fidelity of H₃-H₄ tetramer inheritance has
411 minimal consequences for heritability of the silenced state and may affect heritability of the
412 expressed state in some contexts. These findings raised doubts regarding the model in which
413 histones are significant carriers of epigenetic memory in *S. cerevisiae*. As such, future studies
414 that continue to examine histone-based memory models will be complemented by studies on
415 other possible mechanisms of transcriptional memory.

416

Materials and Methods

Yeast strains

The strains and oligonucleotides used in this study are listed in Supplementary Files 1 and 2, respectively. All strains were derived from the W303 background. CRASH assay strains, which contained *HMR α* , *hmr α 2 Δ ::cre*, *ura3 Δ ::loxP::yEmRFP:tCYC1:KanMX:loxP:yEGFP:tADH1* or *hml α 2 Δ ::cre*, *ura3 Δ ::loxP::yEmRFP:tCYC1:HygMX:loxP:yEGFP:tADH1* were generated as described previously (Dodson & Rine 2015). FLAME assay strains were generated with the following approach. To generate *hml α 2 Δ ::yEmRFP*, a *K. lactis* *URA3* swap was performed to replace the α 2 coding sequence with *yEmRFP* coding sequence. The *hml α 2 Δ ::yEmRFP* fwd/rev primers were used for integration of *yEmRFP* in the final step. To generate *HMR α* , *hmr α 2 Δ ::yEGFP*, a fragment spanning the X region to the Z1 region of *hml α 2 Δ ::yEGFP* was amplified using *hml α 2 Δ ::yEGFP* fwd/rev primers and swapped into *HMR α* .

To delete DNA corresponding to nucleosomes at *HMR α* and *HML α* , CRISPR/Cas9 was employed as previously described (Lee et al. 2015). Each deletion or repair fwd/rev primer set contained two partially overlapping primers that were amplified by PCR prior to use. The *HMR-E*-proximal sgRNA was used to induce Cas9 cutting between the *HMR-E* silencer and *cre*, and N14 to N12 deletion fwd/rev was used to delete DNA corresponding to two nucleosomes in this region. This sgRNA and oligo set was also used to convert sN12 to sN10 in the FLAME strain background. The *HMR-I*-proximal sgRNA, which cuts between the *HMR-I* silencer and *cre*, was used with N14 to N10 deletion fwd/rev (to convert N14 to N10, and sN12 to sN8) or with N14 to N9 deletion fwd/rev (to convert N14 to N9). For *HML α* , the *HML-E*-proximal sgRNA was used to induce Cas9 cutting between the *HML-I* silencer and *cre*, and used with N22 to N19a

deletion fwd/rev (to convert N22 to N19a) or N22 to N16a deletion fwd/rev (to convert N22 to N16a). The *HML-I*-proximal sgRNA was used to induce Cas9 cutting between the *HML-E* silencer and *cre*, and was used with N22 to N19b deletion fwd/rev (to convert N22 to N19b) or N22 to N16c deletion fwd/rev (to convert N22 to N16c) or N22 to N13c deletion fwd/rev (to convert N22 to N13c). Deletions were confirmed by junction primers and sequencing. To generate mutants with combinations of nucleosome set deletions, CRISPR/Cas9 technology was applied (as described above) to strains with one nucleosome set deletion already made.

To generate *dpb3Δ*, the *DPB3* sgRNA was used with Cas9 to cut within *DPB3* and *DPB3* deletion fwd/rev was used to delete the coding sequence. To generate *mcm2-3A*, the *MCM2* sgRNA was used with Cas9 to cut 244bp into the *MCM2* coding sequence and *mcm2-3A* repair fwd/rev was used to generate the appropriate point mutations (Y79A Y82A Y91A). Mutations were confirmed by sequencing.

Colony growth and imaging

To generate colonies for analysis by the CRASH assay, RFP-expressing cells were diluted and plated at a density of ~10 cells/plate (CSM-Trp (Sunrise Science Products, San Diego, CA), 1% agar). After 5 days of growth, colonies were imaged using a Leica M205 FA fluorescence stereomicroscope (Leica Camera AG, Wetzlar, Germany) equipped with a Leica DFC3000G CCD camera, a Leica PLANAPO 0.63x objective, ET RFP filter (Leica 10450224), ET GFP filter (Leica 10447408), and Leica Application Suite X (LAS X) imaging software. At least ten colonies were imaged per genotype.

461 **Live-cell imaging**

462 Cells were grown to saturation in CSM (Sunrise Science Products) at 30°C overnight.
463 These cells were then back-diluted in 5 ml CSM and grown to mid-log phase over 6 hours.
464 500µl was transferred to a microfuge tube and sonicated at 20% for 15 seconds (Branson
465 Ultrasonics Digital Sonifier 100-132-888R with Sonicator Tip 101-135-066R) (Branson
466 Ultrasonics, Fremont, CA) to break up clumps of cells. 5 µl of sonicated cells were spotted onto
467 a CSM plate (1% agar) and allowed to soak into the agar. When dry, a sterile spatula was used
468 to cut a 1 cm × 1 cm agar square surrounding the cell patch. The square was lifted out of the
469 plate, inverted, and placed in a 35 mm glass bottom dish (Thermo Scientific 150682) (Thermo
470 Fisher Scientific, Waltham, MA). Cells were imaged using a Zeiss Z1 inverted fluorescence
471 microscope with a Prime 95B sCMOS camera (Teledyne Photometrics, Tucson, AZ), Plan-
472 Apochromat 63x/1.40 oil immersion objective (Zeiss, Oberkochen, Germany), filters, MS-2000
473 XYZ automated stage (Applied Scientific Instrumentation, Inc., Eugene, OR), and Micro-
474 Manager imaging software (Open Imaging, San Francisco, CA). Given that cells were pressed
475 between the agar and glass, the cells were all in the same focal plane and Z-stacks were not
476 used.

477 For time-lapse microscopy (i.e. Figure 2D), samples were kept at 30°C and humidified
478 with a P-Set 2000 Heated Incubation Insert (PeCon, Erbach, Germany). Time-lapse
479 experiments involved brightfield and fluorescence imaging of 16 different fields per sample,
480 and images were taken every 10 minutes for 10 hours. Subsequent analysis of cell divisions was
481 done in ImageJ (NIH, Bethesda, MD). To measure epigenetic switching rates in the FLAME
482 assay, cell divisions and switching events were manually counted and the counter was blind to

the genotype (single-blind study). This counting was performed only on cells that could be clearly distinguished from each other. If a mother and daughter cell pair switched simultaneously, we counted this as one switching event that probably appeared as two events due to the lag time in yEGFP expression or degradation.

Flow cytometry

To measure fluorescence intensities per cell in the CRASH and FLAME assays, a BD LSR Fortessa cell analyzer (BD Biosciences, San Jose, CA) with a FITC filter (for GFP) and a PE-TexasRed filter (for RFP) was used. Subsequent analysis was performed with FlowJo software.

For quantification of silencing-loss rates in the CRASH assay (Figure 1E and 3B), cells were first streaked out to form single colonies. Six colonies per genotype were added to CSM-Trp media (Sunrise Science Products) in a 96-well plate (Corning CLS3788) (Corning Inc., Corning, NY) and grown to saturation overnight in an incubating microplate shaker (VWR 12620-930) (VWR International, Radnor, PA) at 30°C. These samples were then back-diluted and grown to mid-log phase over 6 hours. GFP and RFP expression were then analyzed by flow cytometry ($n > 4000$ cells per sample). Distinct populations of RFP⁺ GFP⁻ (which had not lost silencing), RFP⁺ GFP⁺ (which had recently lost silencing), and RFP⁻ GFP⁺ (which had lost silencing less recently) were observed. The apparent silencing-loss rate was calculated as the number of RFP⁺ GFP⁺ cells divided by the number of RFP⁺ GFP⁺ cells and RFP⁺ GFP⁻ cells. Measurements from independent cultures were considered as biological replicates.

For calculating the frequency of silenced and expressed cells at equilibrium in the FLAME assay, cells were first streaked out to generate single colonies. Three colonies per

genotype were added to CSM media in a 96-well plate and grown to saturation overnight. These samples were then serially back-diluted in CSM media in 96-well plates and grown at 30°C. After twelve hours, the serial dilutions had a range of cell densities; the dilution that was closest to ~1 O.D. was again back-diluted in CSM media and grown at 30°C for another 12 hours. At this point, wells close to ~1 O.D. contained cells that had been growing at log-phase for approximately 24 hours. These cells were analyzed by flow cytometry. Because three populations were analyzed per genotype, the most representative profiles of silenced and expressed cells were used for figures. We considered these populations as biological replicates.

To calculate GFP expression levels in expressed cells in the FLAME assay, cells were streaked out for single colonies and three colonies per genotype were grown overnight in CSM + 5 mM Nicotinamide (NAM) (Sigma-Aldrich, St. Louis, MO). These samples were then back-diluted in CSM + 5 mM NAM and grown at 30°C for 12 hours. Samples at ~1 O.D. were analyzed by flow cytometry. For Figure 2-figure supplement 3, the most representative profiles of the three profiles generated per strain were shown. For Figure 4-figure supplement 3, the geometric mean intensity of GFP per cell (excluding cells that formed a smaller, artifactual peak at a lower GFP intensity) was calculated for each population using FlowJo software.

Independent cultures were considered as biological replicates.

FACS was utilized in the FLAME assay to calculate switching rates between epigenetic states in Figure 4. To perform this experiment, cells from each genotype were serially diluted in CSM media and grown at 30°C. After 12 hours, dilutions closest to ~1 O.D. were sorted into GFP- and GFP+ populations using a BD FACS Aria Fusion cell sorter (BD Biosciences) equipped with a FITC filter for GFP. Gates were calibrated from *SIR*⁺ (JRY11474) and *sir4Δ* (JRY11496)

cells. For each sample, 150,000 GFP- cells were sorted into one tube and 30,000 GFP+ cells were sorted into another. Each sorted population was divided evenly into three populations and grown in CSM in a 96-well plate at 30°C. Serial back-dilutions were used to maintain constant log-phase growth over two days. Time-points were taken by removing a fraction of cells from each population and fixing them in a 4% paraformaldehyde solution (4% Paraformaldehyde, 3.4% Sucrose) for 15 minutes at room temperature. Fixed cells were resuspended in GFP fix buffer (100 mM KPO₄ pH 7.4, 1.2 M Sorbitol) and kept at 4°C. Once the experiment was complete, fixed cells from different time-points were analyzed by flow cytometry (n > 500 cells per sample) and analyzed by FlowJo software. The percent of GFP+ cells for each sample over time is shown in Figure 4B and 4E. Because the initial sorting event required ~20 minutes per sample, the time of initial sorting (t = 0 hrs) was different between samples; this made the time points between samples slightly staggered as seen in Figure 4B and 4E. Because cells were divided into subpopulations after the initial sorting, these subpopulations were considered as technical replicates.

Switching rate calculation from cell sorting

The following equations were used to model the dynamics of switching rates between epigenetic states in *sir1Δ*. We considered the balance of GFP+ and GFP- cells over time, and assumed that the birth and death rates of the two populations are similar. Combining the balances and introducing the ratio variable x , we can derive the following equation that describes how a population of GFP+ cells and GFP- cells would move towards equilibrium over time:

549

$$\left(\frac{1}{k_{ON} + k_{OFF}}\right) \frac{dx_{ON}}{dt} + x_{ON} = \frac{k_{ON}}{k_{ON} + k_{OFF}}$$

550

551 k_{ON} is the loss rate per hour, k_{OFF} is the establishment rate per hour, x_{ON} is the fraction of

552 GFP+ cells at a given time, and t is time. Solving the differential equation for x_{ON} yields:

553

$$x_{ON} = \frac{k_{ON}}{k_{ON} + k_{OFF}} \left(1 - e^{-\frac{t}{k_{ON} + k_{OFF}}}\right) \text{ or } x_{ON} = \frac{k_{ON}}{k_{ON} + k_{OFF}} \left(1 - e^{-\frac{t}{k_{ON} + k_{OFF}}}\right) + e^{-\frac{t}{k_{ON} + k_{OFF}}}$$

554

555 if $x_{ON} = 0$ at $t = 0$

555 if $x_{ON} = 1$ at $t = 0$

556

557 Therefore, the following equations were used to model switching rates between epigenetic
558 states from data in Figure 4B and 4E.

559

560 Sorting silenced cells (Figure 4B):

561

$$x_{ON} = \frac{k_{ON}}{k_{ON} + k_{OFF}} \left(1 - e^{-\frac{t}{k_{ON} + k_{OFF}}}\right)$$

563

564 Sorting expressed cells (Figure 4E):

565

$$x_{ON} = \frac{k_{ON}}{k_{ON} + k_{OFF}} \left(1 - e^{-\frac{t}{k_{ON} + k_{OFF}}}\right) + e^{-\frac{t}{k_{ON} + k_{OFF}}}$$

566

The `nls()` function in R was used to provide a nonlinear least squares estimate of the unknown variables k_{ON} and k_{OFF} for each genotype, and 95% confidence intervals for estimates. With this approach, each genotype had an estimated k_{ON} and k_{OFF} from sorting silenced cells and an estimated k_{ON} and k_{OFF} from sorting expressed cells. Since sorting silenced cells subsequently allowed for observation of more loss-of-silencing events, the k_{ON} rates from those data were considered more accurate and used in Figure 4C. Similarly, the k_{OFF} rates calculated from sorting expressed cells were used in Figure 4F.

Because each population of sorted cells was evenly divided into three subpopulations, each genotype has three calculated values for the percent of GFP+ cells at each given time point after sorting. The nonlinear least squares estimate was made by drawing a best fit line through all data points for a given genotype, effectively combining the values of all subpopulations. The quality of the fit was calculated using the `confint2()` function and represented as 95% confidence intervals for k_{ON} values in Figure 4C and k_{OFF} values in Figure 4F. An alternative approach involved drawing a best fit line for each individual subpopulation to give three k_{ON} values and three k_{OFF} values for each genotype and averaging these values to get a single k_{ON} value and k_{OFF} value for each genotype, with error bars representing a standard deviation. Though we also performed this latter analysis method, we favor the former analysis method because it incorporates how well the data fit the nonlinear least squares estimate. Notably, both analysis methods gave similar k_{ON} and k_{OFF} values.

The generation time of *DPB3 MCM2* (JRY11471) was 1.96 hours in CSM media at 30°C. To convert k_{ON} and k_{OFF} as rates per hour to rates per generation, we multiplied these

variables by the generation time. Similar generation times were observed for all replisome mutants.

MNase-Seq

Cells were grown to saturation overnight in 5 mL CSM at 30°C. The following day, these cells were back-diluted to ~0.1 O.D. in 50 ml CSM and grown at 30°C for 5 hours. Cells were then centrifuged and washed twice in 500 µl SKC buffer (1.2 M Sorbitol, 100 mM KH₂PO₄, 0.5 mM CaCl₂, 7 mM β-mercaptoethanol) and then resuspended in 100 µl SKC buffer. Cells were incubated at 37°C for 15 minutes, then 30 µl of 1mg/mL Zymolyase-100T (MP Biomedicals, LLC, Solon, OH) was added for a final concentration of 0.23 mg/ml Zymolyase-100T and incubated at 37°C for 15 minutes. All subsequent steps were performed on ice. Once spheroplasting was complete, cells were spun at 3k RPM for 3 minutes at 4°C. Cells were washed twice in 500 µl SPC buffer (1 M Sorbitol, 20 mM PIPES pH 6.3, 0.1 mM CaCl₂, with Roche cOMplete protease inhibitors (Sigma)) and spun at 2k RPM for 3 minutes at 4°C between washes. Cells were resuspended in 250 µl SPC buffer, and this solution was gently mixed with 250 µl freshly prepared Ficoll buffer (9% Ficoll, 20 mM PIPES pH 6.3, 0.5 mM CaCl₂) to lyse the cell membranes.

Nuclei were then pelleted by centrifugation at 10k RPM for 20 minutes at 4°C. Nuclei were washed twice in 500 µl SPC and spun at 8k RPM for 3 minutes at 4°C between washes. Washed nuclei were subsequently resuspended in 250 µl SPC and CaCl₂ was added to a final concentration of 2mM CaCl₂. Nuclei were incubated for 5 minutes at 37°C, then 20 units of Worthington MNase was added (Worthington Biochemical Corporation, Lakewood, NJ). Nuclei

were incubated for 15 minutes at 37°C. MNase activity was quenched by addition of EDTA to a final concentration of 10 mM EDTA. Nuclei were centrifuged at 3.7k RPM for 5 minutes at 4°C. The nucleosome-containing supernatant was subsequently removed and DNA and RNA were purified using a Qiagen spin column. RNase A (Sigma) was added to a final concentration of 1 mg/ml RNase A and incubated for 2 hours at 37°C. DNA was then purified using a Qiagen spin column. MNase libraries were constructed with NEBnextUltra II library preparation kit (New England Biolabs, Ipswich, MA) and sequenced on an Illumina HiSeq4000 (Illumina, San Diego, CA) as 100 bp paired-end reads.

Reads were mapped to the *Saccharomyces cerevisiae* S288C genome (GenBank accession number GCA_000146045.2) using Bowtie2 (Langmead and Salzberg, 2012). Mapped reads between 140 bp and 180 bp in length were used in all further analysis to ensure mononucleosome resolution. The midpoint for each read was calculated and midpoints were stacked in a histogram. Finally, a 25 bp rolling mean was used to smooth out the resulting nucleosome peaks. All sequences and processed data files have been deposited in the NCBI Gene Expression Omnibus archive under accession number GSE136897.

Acknowledgements

We thank Anne Dodson for providing strains and genetic tools that were integral to this study. We also thank the UC Berkeley Flow Cytometry facility, especially Hector Nolla, for use of flow cytometers. This work used the Vincent J. Coates Genomics Sequencing Laboratory at UC Berkeley, supported by NIH S10 OD018174 Instrumentation Grant. We are grateful to Marc Fouet for help with microscopy and modeling switching rates. We thank Albert Serra-Cardona for discussions on replisome factors and histone inheritance patterns. Finally, we thank Rine laboratory members for thoughtful discussions, especially Gavin Schlissel, Davis Goodnight, Molly Brothers, Ryan Janke, Eliana Bondra, and Delaney Farris.

Competing Interests

The authors declare that no competing interests exist.

641 Main Figures

642 Figure 1: Chromatin Domain Size Did Not Affect Silencing-Loss Rates. (A) Schematic of the

643 Cre-Reported Altered States of Heterochromatin (CRASH) assay (Dodson & Rine 2015).

644 *HMR α ::cre* contains the *E* and *I* silencers, the $\alpha 1$ gene, and a *cre* transgene. Transient loss of

645 silencing at *HMR α ::cre* causes Cre-mediated recombination of *loxP* sites in a *RFP-GFP* cassette.

646 This process creates a permanent, heritable switch from RFP to GFP expression. (B) Diagram of

647 nucleosomes in *HMR α ::cre*. Fourteen nucleosomes were present in full-length *HMR α ::cre*,

648 which we term Strain N14 (JRY11471). Combinations of nucleosomal DNA were deleted to

649 change the size of *HMR α ::cre*; the smallest size was seven nucleosomes (Strain N7) (JRY11540).

650 Nucleosome positions were determined by MNase-seq as shown in Figure 1-figure supplement

651 1. (C) Schematic of how random segregation of parental H₃-H₄ tetramers to daughter

652 chromatids could cause silencing loss. Under the model that inheritance of a single marked H₃-

653 H₄ tetramer to a daughter chromatid would be sufficient to propagate the silenced state, the

654 chance that a daughter chromatid inherits no parental tetramers and loses the silenced state

655 would be $0.5^{(\text{the number of nucleosomes in the chromatin domain})}$. Parental nucleosomes

656 contain inherited H₃-H₄ tetramers, whereas new nucleosomes contain newly synthesized H₃-

657 H₄ tetramers. Hypothetical chromatin domains of different sizes are provided for comparison.

658 (D) Expected loss-of-silencing rates for different sizes of *HMR α ::cre*. (E) Representative CRASH

659 colonies for Strains N14 through N7. Because loss of silencing leads to a heritable switch from

660 RFP to GFP expression, progeny of a cell that loses silencing will form a GFP sector; the

661 frequency of sectors in a colony represents the frequency at which that strain loses silencing.

662 Scale bar, 2 mm. (F) Quantification of apparent silencing-loss rates, as described in *Materials*

663 *and Methods*. Data are means \pm SD ($n = 6$ independent cultures). ANOVA and Tukey tests were
664 used to test statistical significance. Only strains N10 and N7 were significantly different ($p <$
665 0.05) than N14. Data are presented as a scatter plot in Figure 1-figure supplement 2.

666

667 Figure 2: Chromatin Domain Size Did Not Affect Silencing-Loss Rates in *sir1* Δ . (A) Diagram of
668 the FLuorescent Analysis of Metastable Expression (FLAME) assay. In a *sir1* Δ background, *GFP*
669 replaced the $\alpha 2$ gene so that transcriptional activity of *HMR* α ::*GFP* could be monitored at the
670 single-cell level (JRY11478). Loss-of-silencing events were observed in dividing cells by using
671 time-lapse microscopy. Scale bar, 5 μ m. Establishment-of-silencing events were also observed
672 (see Video 1). Silencing defects in different *sir* mutants are shown by microscopy in Figure 2-
673 figure supplement 1 and by flow cytometry in Figure 2-figure supplement 2. (B) Diagram of
674 nucleosomes in *HMR* α ::*GFP* as defined by MNase-Seq (Figure 2-figure supplement 3). Twelve
675 nucleosomes were present in full-length *HMR* α ::*GFP* (Strain sN12) (JRY11478). Combinations
676 of nucleosomal DNA were deleted to change the size of the *HMR* α ::*GFP* locus; the smallest
677 version of the locus contained six nucleosomes (Strain sN6) (JRY11547). (C) Expected loss-of-
678 silencing rate from random segregation of H3-H4 tetramers to daughter chromatids. See the
679 legend of Figure 1 for a description of how these expected rates were calculated. (D) Observed
680 loss-of-silencing rates using the FLAME assay. Cell divisions were monitored by time-lapse
681 microscopy ($n > 900$ cell divisions per genotype). Silencing-loss rates were not significantly
682 different (Yates chi-square test, $p > 0.05$ for all pairwise comparisons). (E) Observed
683 establishment-of-silencing rates using the FLAME assay ($n > 110$ cell divisions per genotype).
684 Silencing establishment rates were not significantly different (Yates chi-square test, $p > 0.05$

for all pairwise comparisons). These strains showed similar frequencies of silenced and expressed cells as measured by flow cytometry in Figure 2-figure supplement 4. Error bars represent 95% confidence intervals.

Figure 3: Replisome mutants exhibited higher silencing-loss rates in the CRASH assay. (A) Representative CRASH colonies for *DPB3 MCM2* (JRY11471), *dpb3Δ MCM2* (JRY11562), *DPB3 mcm2-3A* (JRY11591), and *dpb3Δ mcm2-3A* (JRY11592). Scale bar, 1 mm. (B) Quantification of apparent silencing-loss rates of strains in (A), as described in *Materials and Methods*. Data are means \pm SD (n = 6 independent cultures). ANOVA and Tukey tests were used to test statistical significance. *DPB3 MCM2* was significantly different than *dpb3Δ MCM2* and *DPB3 mcm2-3A* ($p < 0.05$ each), and *dpb3Δ mcm2-3A* was significantly different than *dpb3Δ MCM2* and *DPB3 mcm2-3A* ($p < 0.05$ each).

Figure 4: Replisome mutants exhibited defects in epigenetic inheritance in the FLAME assay. (A) FACS-based approach to measure switching rates of *HMR α ::GFP* in *sir1Δ*. Populations of silenced cells were isolated and allowed to divide; as silencing loss occurred, the percentage of expressed cells in the population increased. The frequencies of fluorescence intensity per cell at equilibrium are shown in Figure 4-figure supplement 1. (B) For *DPB3 MCM2* (blue) (JRY11471), *dpb3Δ MCM2* (black) (JRY11550), *DPB3 mcm2-3A* (green) (JRY11589), and *dpb3Δ mcm2-3A* (red) (JRY11590), silenced cells were isolated at t = 0 hrs, allocated into three separate populations each, and monitored over time. At each time-point, the percentage of expressed cells in each population was determined by flow cytometry (for an example, see

Figure 4-figure supplement 2). (C) Silencing-loss rates calculated from (B), as explained in *Materials and Methods*. (D) Silencing-loss rates calculated by monitoring dividing cells with time-lapse microscopy ($n > 550$ cell divisions per genotype). (E) Similar to (B), except expressed cells were sorted and monitored over time. (F) Silencing-establishment rates calculated from (E), as explained in *Materials and Methods*. (G) Silencing-establishment rates calculated by monitoring dividing cells with time-lapse microscopy ($n > 100$ cell divisions per genotype). GFP expression levels in expressed cells were calculated by flow cytometry and shown in Figure 4-figure supplement 3. Error bars represent 95% confidence intervals. Two-tailed t-tests were used in statistical analysis of switching rates by sorting, and Yates chi-square tests were used for microscopy ($*p < 0.05$).

Figure 5: Chromatin domain size did not strongly affect epigenetic switching rates in replisome mutant backgrounds. (A) Diagram of nucleosomes in *HMR α ::GFP*, as seen in Figure 2B. As before, combinations of nucleosomal DNA were deleted to change the size of *HMR α ::GFP*; the largest size contained twelve nucleosomes (Strain sN12) (JRY11478) and the smallest size contained six nucleosomes (Strain sN6) (JRY11547). Frequencies of silenced and expressed cells in these strains were measured by flow cytometry and shown in Figure 5-figure supplement 1. (B) Loss-of-silencing rates in the FLAME assay. Replisome mutant strains *DPB3 MCM2* (JRY11478) (white), *dpb3 Δ MCM2* (JRY11550) (grey), and *dpb3 Δ mcm2-3A* (JRY11590) (dark grey) with different numbers of nucleosomes at *HMR α ::GFP* were analyzed by time-lapse microscopy ($n > 300$ cell divisions for each genotype). (C) Establishment-of-silencing rates for the same strains as in (B), calculated by time-lapse microscopy ($n > 80$ cell divisions per

729 genotype). Loss and establishment rates of *DPB3 MCM2* (JRY11478) are identical to those in
730 Figure 2D,E and shown here for convenience. Error bars represent 95% confidence intervals.
731

Figure Supplements

Figure 1-figure supplement 1: Nucleosome set deletions did not affect positions of remaining nucleosomes. MNase-Seq was performed on strains with different sizes of *HMR α ::cre*. Midpoints of nucleosome-sized fragments were calculated, plotted, and smoothed.

Figure 1-figure supplement 2: Chromatin domain-size of *HMR α ::cre* had minimal effects on silencing. Data represent means of apparent silencing-loss rates (n = 6 independent cultures) from Figure 1F, presented as a scatter plot.

Figure 1-figure supplement 3: *HML α ::cre* contained 22 nucleosomes. MNase-Seq was performed on the strain with full-length *HML α ::cre* (JRY11259). Midpoints of nucleosome-sized fragments were calculated, plotted, and smoothed.

Figure 1-figure supplement 4: Chromatin domain size of *HML α ::cre* had minimal effects on silencing-loss rates. (A) Diagram of nucleosomes in full-length *HML α ::cre* (N22) (JRY11259) and strains with deletions of nucleosomal DNA. The smallest version of *HML α ::cre* had seven nucleosomes (N7) (JRY11292). (B) Representative CRASH colonies for Strains N22 (JRY11259) through N7 (JRY11292). Scale bar, 2 mm.

Figure 1-figure supplement 5: Chromatin domain size of *HML α ::cre* had minimal effects on silencing-loss rates measured by flow cytometry. (A) Diagram of nucleosomes in *HML α ::cre*, as shown in Figure 1-figure supplement 3. (B) Quantification of apparent silencing-loss rates, as

described in *Materials and Methods*. Data are means \pm SD (n = 6 independent cultures). ANOVA and Tukey tests were used to test for statistical significance. Only strains N13c and N7 were significantly different ($p < 0.05$) than N22. (C) Data from (B), with means of apparent silencing-loss rates presented on a scatter plot.

Figure 2-figure supplement 1: *sir1Δ* cells exhibited metastability at *HMRα::GFP*. Fluorescence images of *HMRα::GFP* strains that were *SIR⁺* (JRY11474), *sir4Δ* (JRY11496), or *sir1Δ* (JRY11478). Cells were grown to log-phase before imaging. Scale bar, 5 μ m.

Figure 2-figure supplement 2: *sir1Δ* cells exhibited metastability at *HMLα::RFP* and *HMRα::GFP*. Distribution of fluorescence intensity per cell as measured by flow cytometry after 24 hours of log-phase growth. (A) *HMLα::RFP* expression was measured in *SIR⁺* (JRY11472), *sir4Δ* (JRY11494), or *sir1Δ* (JRY11476). (B) *HMRα::GFP* expression was measured in *SIR⁺* (JRY11474), *sir4Δ* (JRY11496), or *sir1Δ* (JRY11478). Because very few cells expressed *HMRα::GFP* in *sir1Δ*, zoomed profiles are provided in (C). At least 50,000 cells were analyzed for each strain.

Figure 2-figure supplement 3: *HMRα::GFP* contained 12 nucleosomes. MNase-Seq was performed on the strain with full-length *HMRα::GFP* in *sir1Δ* (JRY11478). Midpoints of nucleosome-sized fragments were calculated, plotted, and smoothed.

Figure 2-figure supplement 4: Chromatin domain size of *HMRα::GFP* in *sir1Δ* did not affect the frequencies of different epigenetic states but did affect GFP expression levels. Distribution of fluorescence intensity per cell as measured by flow cytometry after 24 hours of log-phase growth. (A) *HMRα::GFP* expression was measured in Strains sN12 (JRY11478) through sN6 (JRY11547). (B) Zoomed profiles of flow cytometry profiles in (A). The dashed line indicates the mean fluorescence intensity of expressed cells in sN12, for comparison to the mean-fluorescence-intensity values of other strains. (C) Distribution of fluorescence intensity per cell for cells grown at log for 12 hours in 5 mM Nicotinamide (NAM). NAM inhibits Sir2 activity and causes cells to be fully expressed at *HMR*. Strains sN12 through sN6 were analyzed. The dashed line indicates the mean fluorescence intensity of expressed cells in sN12, for comparison to other strains. Because the smaller peaks at lower fluorescence intensities were not visible in *sir4Δ* (see Figure 2-figure supplement 2), we considered them an artifact of NAM treatment. At least 50,000 cells were analyzed for each strain.

Figure 4-figure supplement 1: Replisome mutants exhibited different frequencies of silenced and expressed cells in *sir1Δ*. Distribution of fluorescence intensity per cell as measured by flow cytometry after 24 hours of log-phase growth. *HMRα::GFP* expression was measured in *DPB3 MCM2* (JRY11471), *dpb3Δ MCM2* (JRY11550), *DPB3 mcm2-3A* (JRY11589), and *dpb3Δ mcm2-3A* (JRY11590). At least 50,000 cells were analyzed for each strain.

Figure 4-figure supplement 2: Flow cytometry profiles of *sir1Δ dpb3Δ mcm2-3A HMRα::GFP* after FACS sorting. Silenced and expressed cells were sorted at t = 0 hrs and allowed to divide

at log-phase. Samples were taken at different time-points and analyzed by flow cytometry. These data correspond to experiments shown in Figure 4B and 4E. At least 700 cells were analyzed for each time-point.

Figure 4-figure supplement 3: *dpb3Δ* exhibited a higher expression level of *HMRα::GFP* in expressed cells. *DPB3 MCM2* (JRY11478), *dpb3Δ MCM2* (JRY11550), *DPB3 mcm2-3A* (JRY11589), and *dpb3Δ mcm2-3A* (JRY11590) were grown at log phase for 12 hours in 5 mM Nicotinamide (NAM) and *HMRα::GFP* expression was measured with flow cytometry. The geometric mean intensity of GFP for each strain was calculated using FlowJo software. Data are means ± SD (n = 3 independent cultures). ANOVA and Tukey tests showed GFP expression levels in *DPB3 MCM2* were significantly different than those seen in *dpb3Δ MCM2*, *DPB3 mcm2-3A*, and *dpb3Δ mcm2-3A* ($p < 0.05$ each). GFP expression in *dpb3Δ MCM2* was not significantly different than *dpb3Δ mcm2-3A* ($p > 0.05$).

Figure 5-figure supplement 1: Chromatin domain size of *HMRα::GFP* did not strongly affect the frequencies of different epigenetic states in replisome mutant backgrounds. Distribution of fluorescence intensity per cell as measured by flow cytometry after 24 hours of log-phase growth. This analysis was performed on *DPB3 MCM2* (JRY11478) (A), *dpb3Δ MCM2* (JRY11550) (B), and *dpb3Δ mcm2-3A* (JRY11590) (C) with different numbers of nucleosomes at *HMRα::GFP*. At least 50,000 cells were analyzed for each strain. Data in (A) corresponds to data in Figure 2-figure supplement 4A.

819

Genotype	Silenced (S)	Expressed (E)	$S \rightarrow E$ (k_{on} , gen^{-1})	$E \rightarrow S$ (k_{off} , gen^{-1})	K_D (E/S)	K_D (k_{on}/k_{off})
<i>DPB3 MCM2</i>	99	1	0.003	0.11	0.01	0.031
<i>dpb3Δ MCM2</i>	96	4	0.014	0.78	0.042	0.019
<i>DPB3 mcm2-3A</i>	91	9	0.018	0.17	0.094	0.107
<i>dpb3Δ mcm2-3A</i>	90	10	0.033	0.5	0.115	0.066

820

821 Table 1: Comparison of epigenetic switching rates and proportion of silenced cells at
822 equilibrium. Data for *DPB3 MCM2* (JRY11471), *dpb3Δ MCM2* (JRY11550), *DPB3 mcm2-3A*
823 (JRY11589), and *dpb3Δ mcm2-3A* (JRY11590) in the FLAME assay was extracted from Figure 4.
824 The percentages of Silenced (S) and Expressed (E) cells at equilibrium were determined from
825 Figure 4B. Silencing-loss rates (k_{on} , gen^{-1}) correspond to data from Figure 4C and silencing-
826 establishment rates (k_{off} , gen^{-1}) correspond to data from Figure 4F.

827

828 Separate Files

829 Video 1: Time-lapse video of inheritance of epigenetic states in the FLAME assay. *HMRα::GFP*
830 *sir1Δ* (JRY11478) cells were grown to log-phase in liquid media and subsequently imaged by
831 time-lapse microscopy. A loss-of-silencing event is visible near the center of the field of view at
832 4 hrs, and an establishment-of-silencing event is visible near the upper-left corner at 5 hrs.

833

834 Supplementary file 1: Table of yeast strains used in this study.

835

836 Supplementary file 2: Table of oligonucleotides used in this study.

837

838 References

839 Alabert, C. et al., 2015. Two distinct modes for propagation of histone PTMs across the cell
840 cycle. *Genes & development*, 29(6), pp.585–590.

841 Audergon, P.N.C.B. et al., 2015. Epigenetics. Restricted epigenetic inheritance of H3K9
842 methylation. *Science*, 348(6230), pp.132–135.

843 Berry, S. et al., 2015. Local chromatin environment of a Polycomb target gene instructs its own
844 epigenetic inheritance. *eLife*.

845 Cheng, T.H. & Gartenberg, M.R., 2000. Yeast heterochromatin is a dynamic structure that
846 requires silencers continuously. *Genes & development*, 14(4), pp.452–463.

847 Cusick, M.E., DePamphilis, M.L. & Wassarman, P.M., 1984. Dispersive segregation of
848 nucleosomes during replication of simian virus 40 chromosomes. *Journal of molecular*
849 *biology*, 178(2), pp.249–271.

850 Dodd, I.B. et al., 2007. Theoretical Analysis of Epigenetic Cell Memory by Nucleosome
851 Modification. *Cell*, 129(4), pp.813–822.

852 Dodson, A.E. & Rine, J., 2015. Heritable capture of heterochromatin dynamics in
853 *Saccharomyces cerevisiae*. *eLife*, 4, p.e05007.

854 Foltman, M. et al., 2013. Eukaryotic Replisome Components Cooperate to Process Histones
855 During Chromosome Replication. *Cell reports*, 3(3), pp.892–904.

856 Gan, H. et al., 2018. The Mcm2-Ctf4-Pol α Axis Facilitates Parental Histone H3-H4
857 Transfer to Lagging Strands. *Molecular cell*, pp.1–16.

858 Gaydos, L.J., Wang, W. & Strome, S., 2014. Gene repression. H3K27me and PRC2 transmit a
859 memory of repression across generations and during development. *Science*, 345(6203),
860 pp.1515–1518.

861 Hansen, K.H. et al., 2008. A model for transmission of the H3K27me₃ epigenetic mark. *Nature*
862 *Cell Biology*, 10(11), pp.1291–1300.

863 Hecht, A. et al., 1995. Histone H3 and H4 N-termini interact with SIR3 and SIR4 proteins: a
864 molecular model for the formation of heterochromatin in yeast. *Cell*.

865 Holmes, S.G. & Broach, J.R., 1996. Silencers are required for inheritance of the repressed state
866 in yeast. *Genes & development*, 10(8), pp.1021–1032.

867 Hoppe, G.J. et al., 2002. Steps in Assembly of Silent Chromatin in Yeast: Sir3-Independent
868 Binding of a Sir2/Sir4 Complex to Silencers and Role for Sir2-Dependent Deacetylation.
869 *Molecular and Cellular Biology*, 22(12), pp.4167–4180.

Hyland, E.M. et al., 2005. Insights into the Role of Histone H₃ and Histone H₄ Core Modifiable Residues in *Saccharomyces cerevisiae*. *Molecular and Cellular Biology*, 25(22), pp.10060–10070.

Iida, T. & Araki, H., 2003. Noncompetitive Counteractions of DNA Polymerase and ISW2/γCHRAC for Epigenetic Inheritance of Telomere Position Effect in *Saccharomyces cerevisiae*. *Molecular and Cellular Biology*, 24(1), pp.217–227.

Imai, S. et al., 2000. Transcriptional silencing and longevity protein Sir2 is an NAD-dependent histone deacetylase. *Nature*, 403(6771), pp.795–800.

Jackson, V., 1988. Deposition of newly synthesized histones: hybrid nucleosomes are not tandemly arranged on daughter DNA strands. *Biochemistry*, 27(6), pp.2109–2120.

Jacobson, R.H. et al., 2000. Structure and Function of a Human TAFII250 Double Bromodomain Module. *Science*, 288(5470), pp.1422–1425.

Kaufman, P.D. & Rando, O.J., 2010. Chromatin as a potential carrier of heritable information. *Current Opinion in Cell Biology*, 22(3), pp.284–290.

Laprell, F., Finkl, K. & Müller, J., 2017. Propagation of Polycomb-repressed chromatin requires sequence-specific recruitment to DNA. *Science*, pp.eaai8266–7.

Lee, M.E. et al., 2015. A Highly Characterized Yeast Toolkit for Modular, Multipart Assembly. *ACS Synthetic Biology*, 4(9), pp.975–986.

Moazed, D., 2011. Mechanisms for the Inheritance of Chromatin States. *Cell*, 146(4), pp.510–518.

Owen, D.J. et al., 2000. The structural basis for the recognition of acetylated histone H₄ by the bromodomain of histone acetyltransferase gcn5p. *The EMBO journal*, 19(22), pp.6141–6149.

Petryk, N. et al., 2018. MCM2 promotes symmetric inheritance of modified histones during DNA replication. *Science*, 3, pp.eaau0294–8.

Pillus, L. & Rine, J., 1989. Epigenetic inheritance of transcriptional states in *S. cerevisiae*. *Cell*, 59(4), pp.637–647.

Prior, C.P. et al., 1980. Incorporation of exogenous pyrene-labeled histone into *Physarum* chromatin: a system for studying changes in nucleosomes assembled in vivo. *Cell*, 20(3), pp.597–608.

Ragunathan, K., Jih, G. & Moazed, D., 2015. Epigenetics. Epigenetic inheritance uncoupled from sequence-specific recruitment. *Science*, 348(6230), p.1258699.

902 Ramachandran, S. & Henikoff, S., 2015. Replicating nucleosomes. *Science Advances*, 1(7),
903 pp.e1500587–e1500587.

904 Reverón-Gómez, N. et al., 2018. Accurate Recycling of Parental Histones Reproduces the
905 Histone Modification Landscape during DNA Replication. *Molecular cell*, 72(2), pp.239–
906 249.e5.

907 Rusché, L.N., Kirchmaier, A.L. & Rine, J., 2002. Ordered nucleation and spreading of silenced
908 chromatin in *Saccharomyces cerevisiae*. *Molecular biology of the cell*, 13(7), pp.2207–2222.

909 Rusché, L.N., Kirchmaier, A.L. & Rine, J., 2003. The establishment, inheritance, and function of
910 silenced chromatin in *Saccharomyces cerevisiae*. *Annual review of biochemistry*, 72,
911 pp.481–516.

912 Schlissel, G. & Rine, J., 2019. The nucleosome core particle remembers its position through
913 DNA replication and RNA transcription. *Proceedings of the National Academy of Sciences of
914 the United States of America*, 116(12), pp.201911943–7.

915 Schwartz, Y.B. et al., 2006. Genome-wide analysis of Polycomb targets in *Drosophila*
916 *melanogaster*. *Nature genetics*, 38(6), pp.700–705.

917 Sogo, J.M. et al., 1986. Structure of replicating simian virus 40 minichromosomes. The
918 replication fork, core histone segregation and terminal structures. *Journal of molecular
919 biology*, 189(1), pp.189–204.

920 Thurtle, D.M. & Rine, J., 2014. The molecular topography of silenced chromatin in
921 *Saccharomyces cerevisiae*. *Genes & development*, 28(3), pp.245–258.

922 Xu, E.Y., Zawadzki, K.A. & Broach, J.R., 2006. Single-Cell Observations Reveal Intermediate
923 Transcriptional Silencing States. *Molecular cell*, 23(2), pp.219–229.

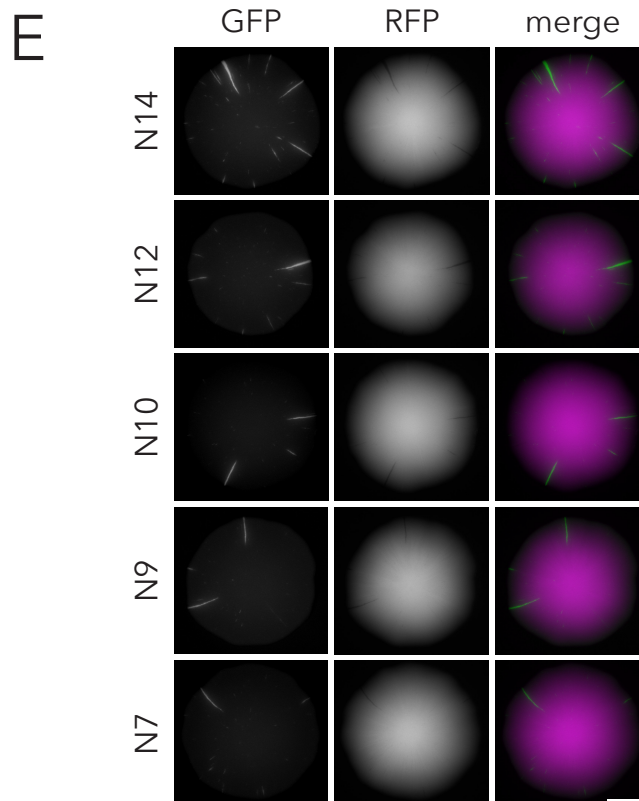
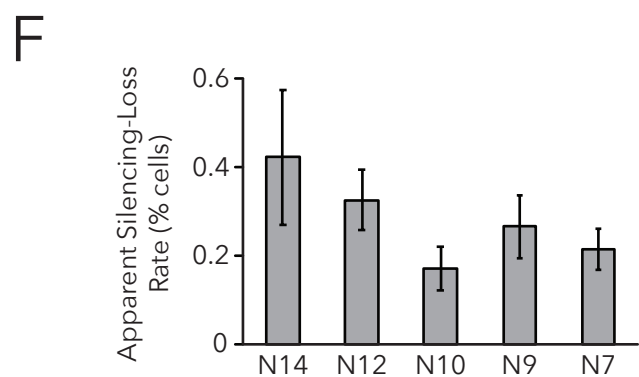
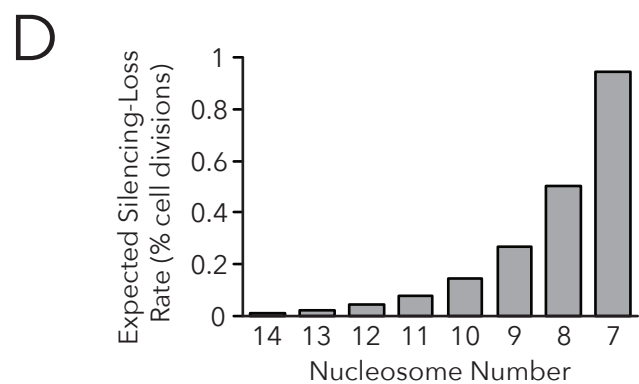
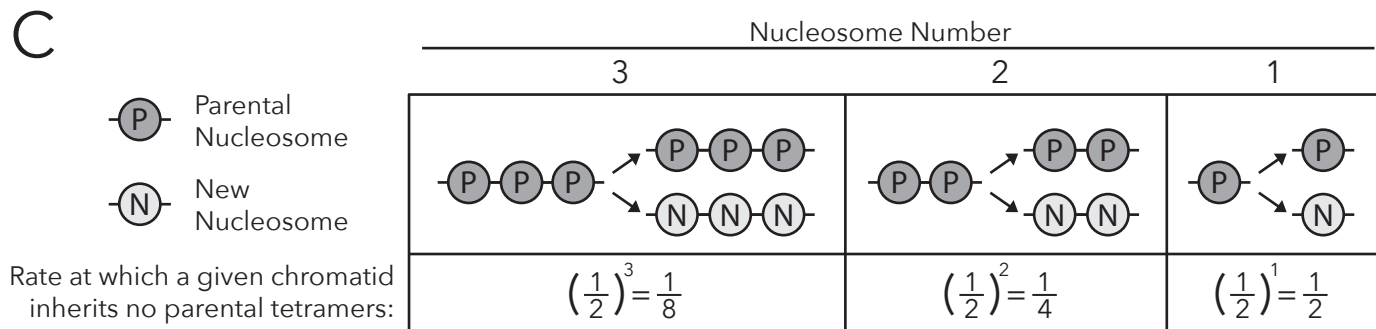
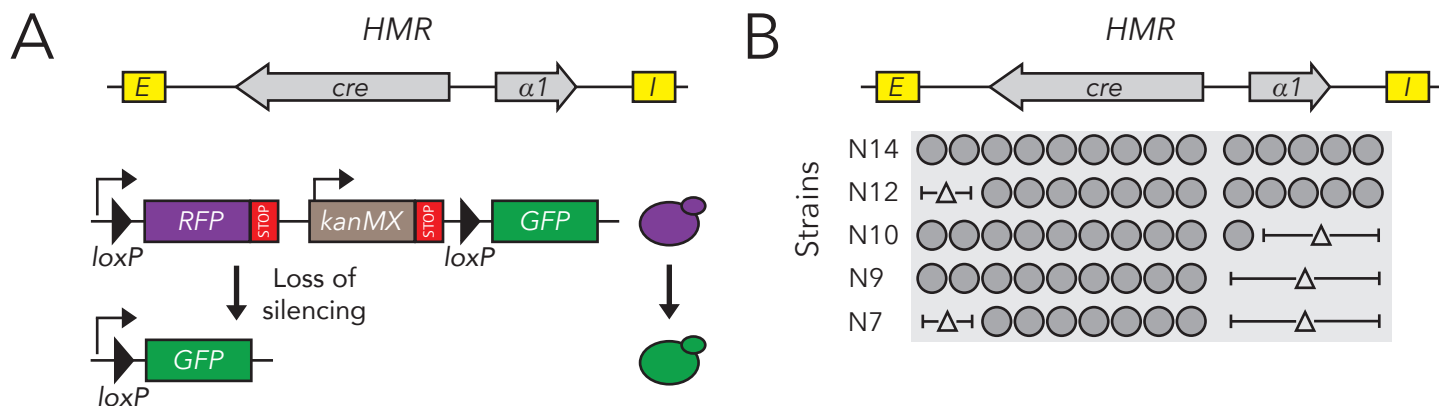
924 Xu, F. et al., 2007. Sir2 deacetylates histone H3 lysine 56 to regulate telomeric heterochromatin
925 structure in yeast. *Molecular cell*, 27(6), pp.890–900.

926 Yang, H. et al., 2017. Distinct phases of Polycomb silencing to hold epigenetic memory of cold
927 in *Arabidopsis*. *Science*, 357(6356), pp.1142–1145.

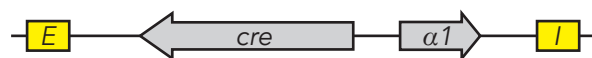
928 Yu, C. et al., 2018. A mechanism for preventing asymmetric histone segregation onto
929 replicating DNA strands. *Science*, pp.eaat8849–8.

930 Zhang, K. et al., 2008. Roles of the Clr4 methyltransferase complex in nucleation, spreading
931 and maintenance of heterochromatin. *Nature structural & molecular biology*, 15(4), pp.381–
932 388.

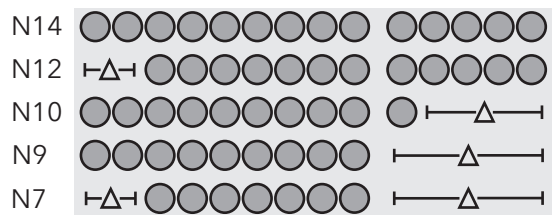
933



HMR

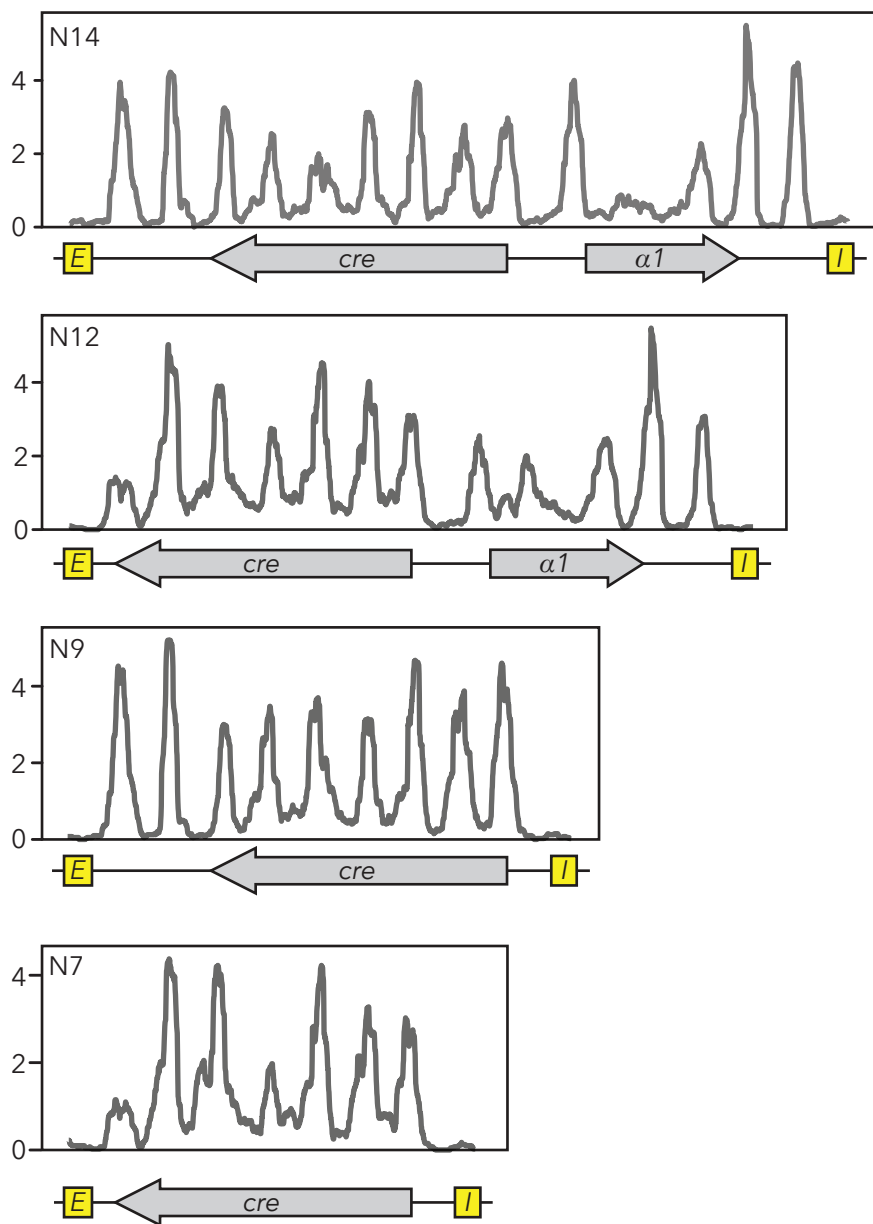


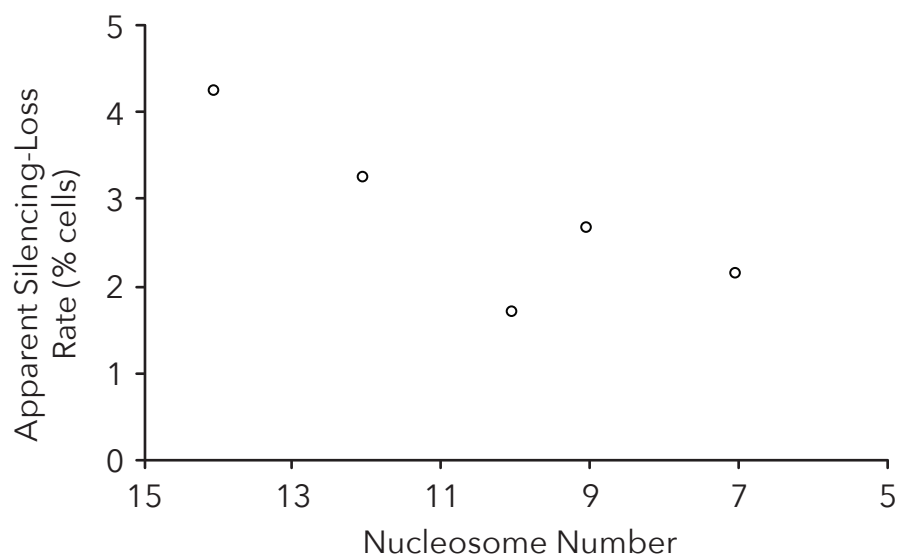
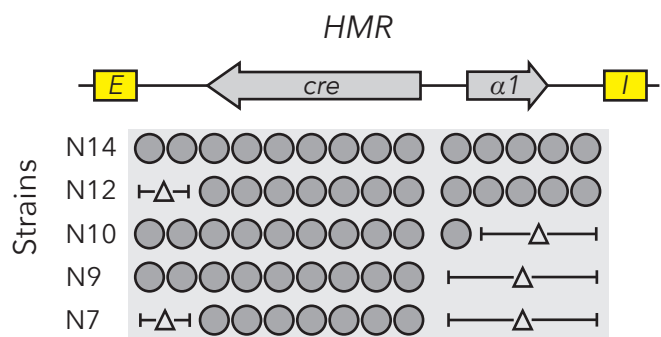
Strains



500 bp

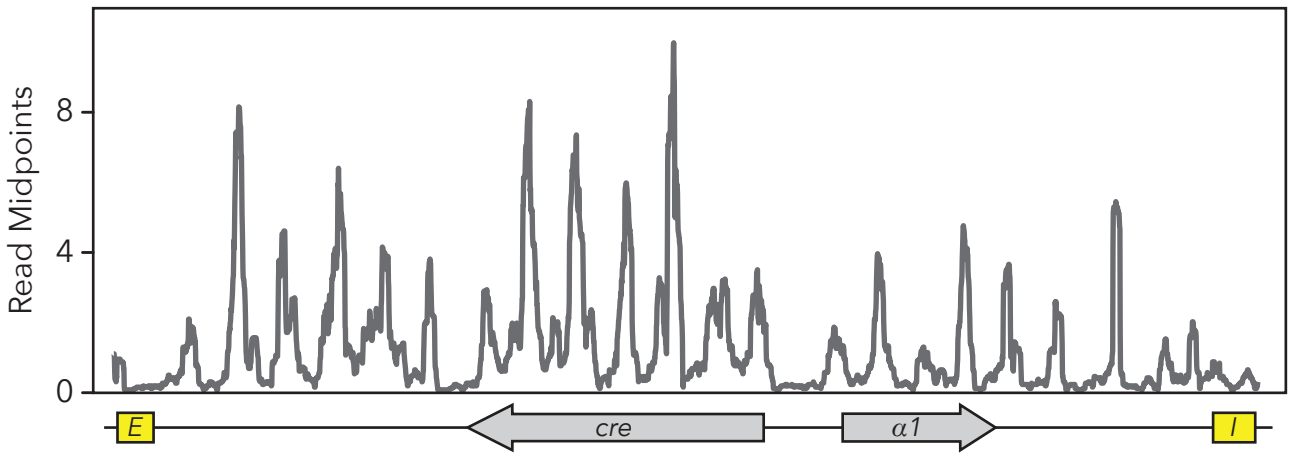
Read Midpoints



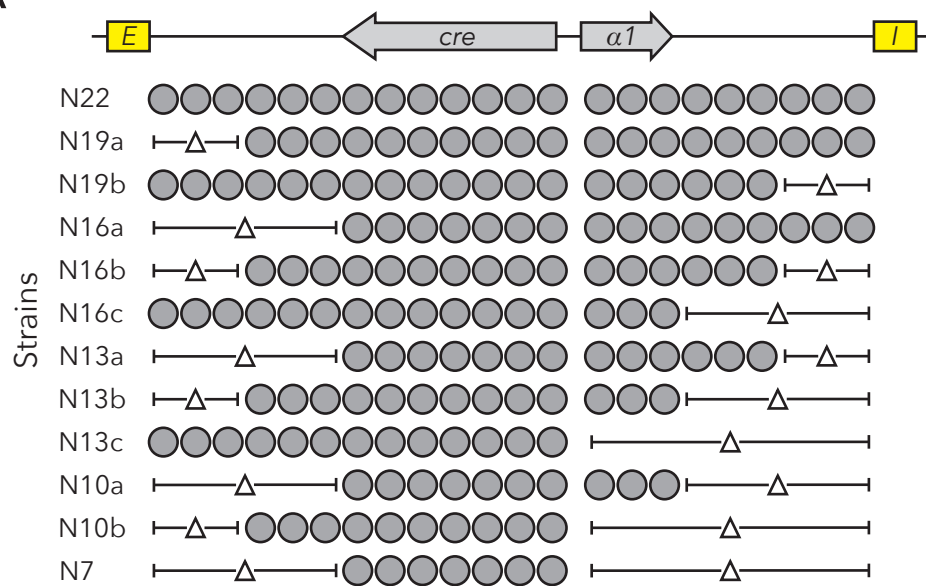


HML

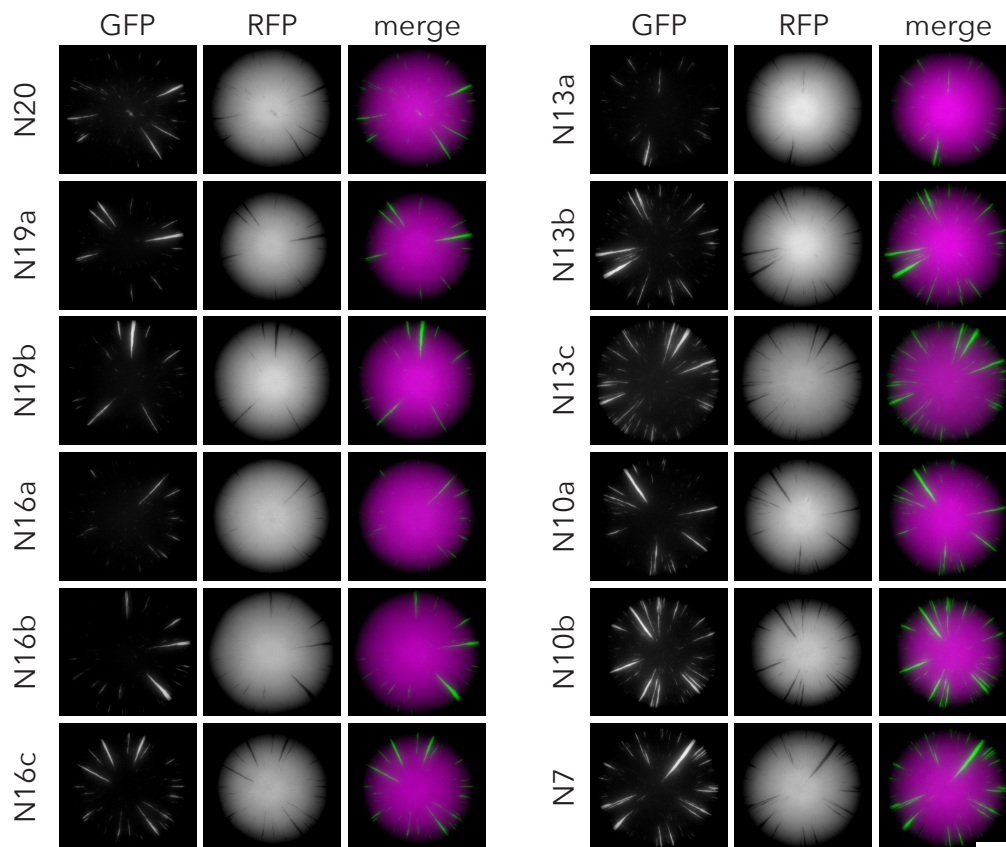
500 bp

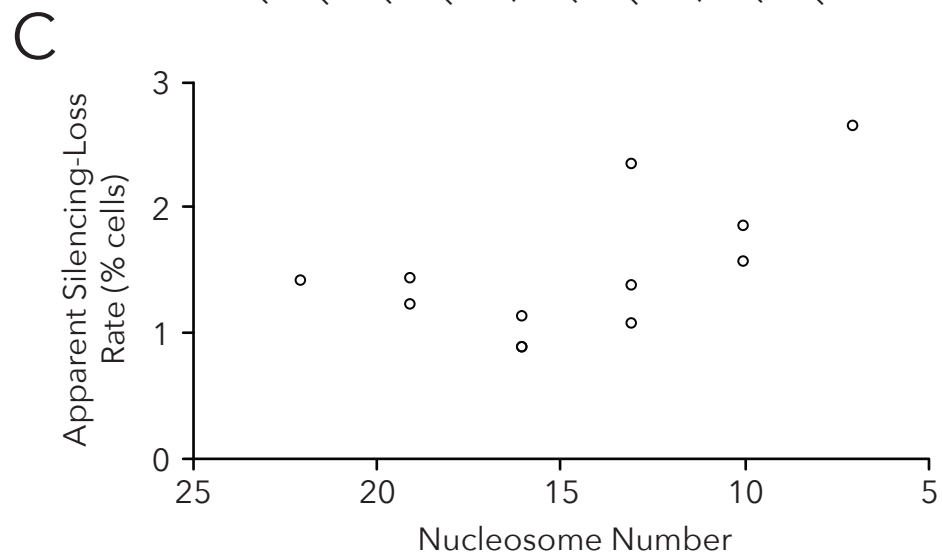
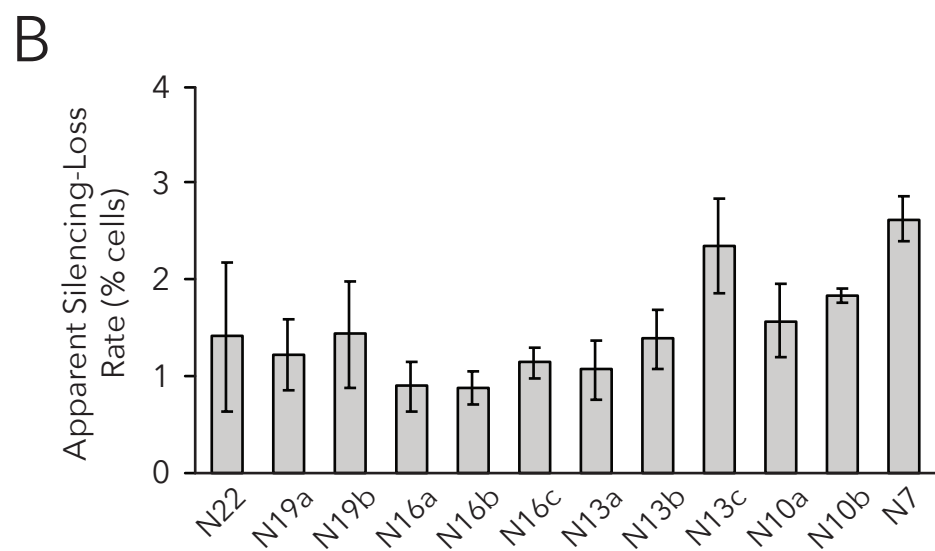
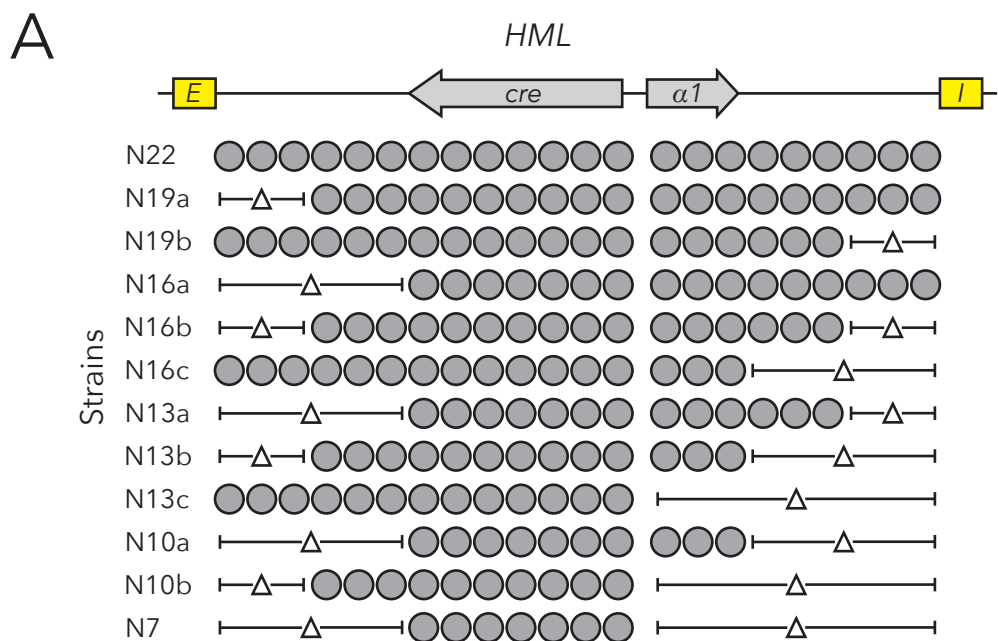


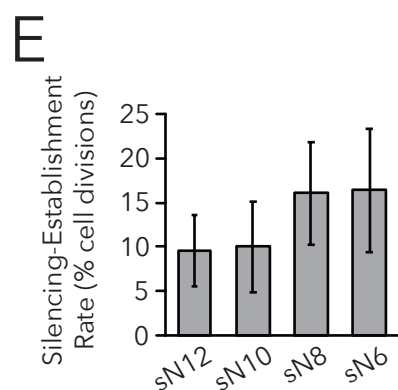
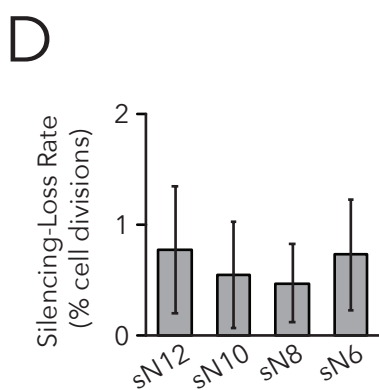
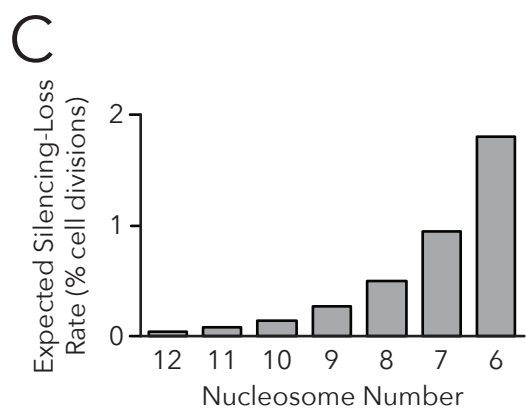
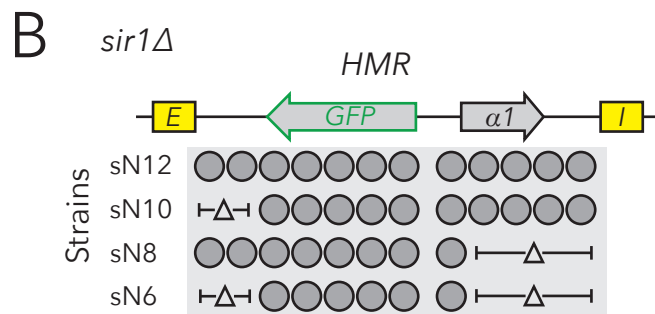
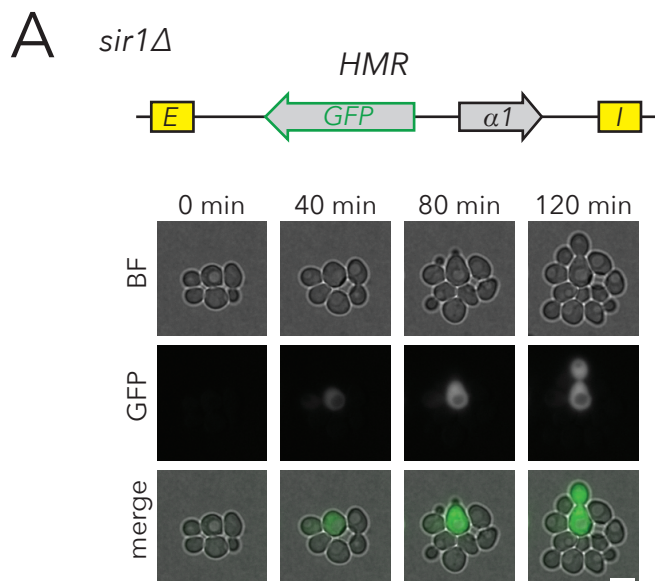
HML

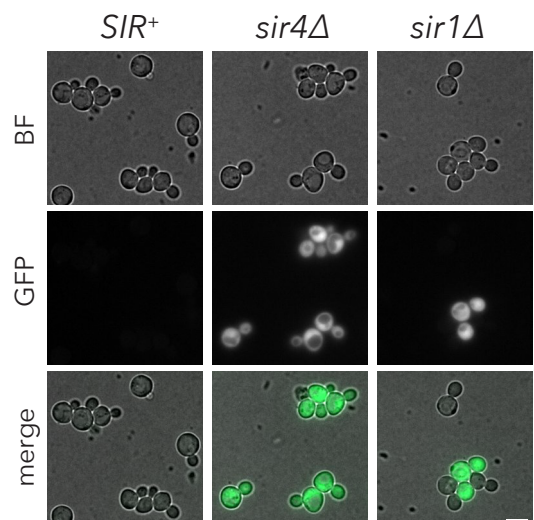


B

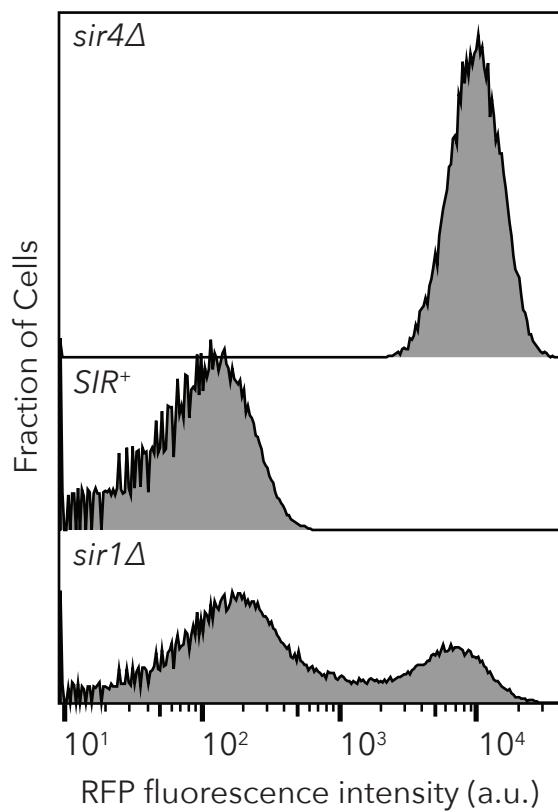




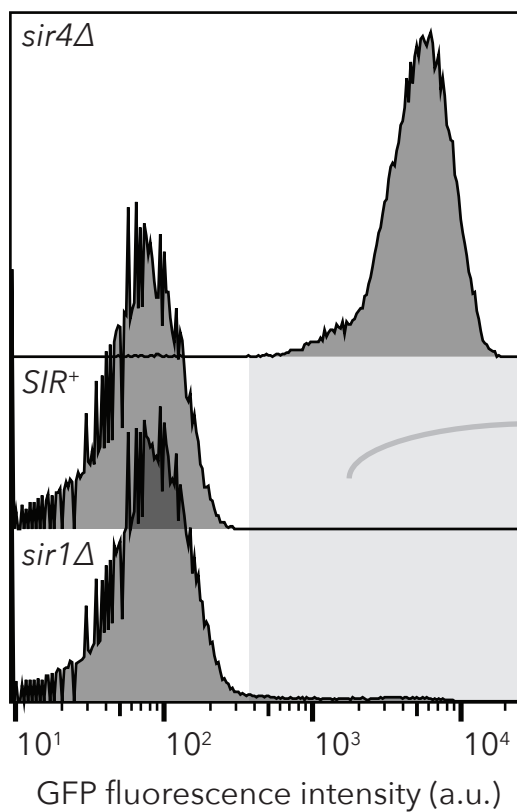




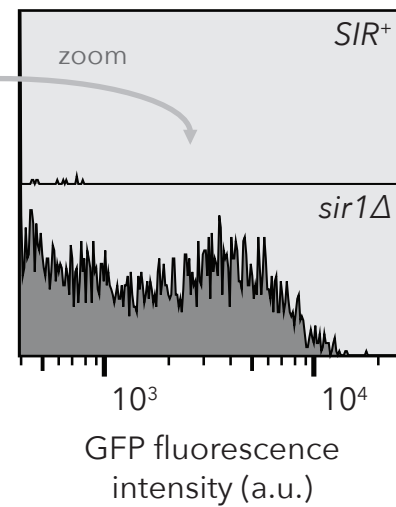
A

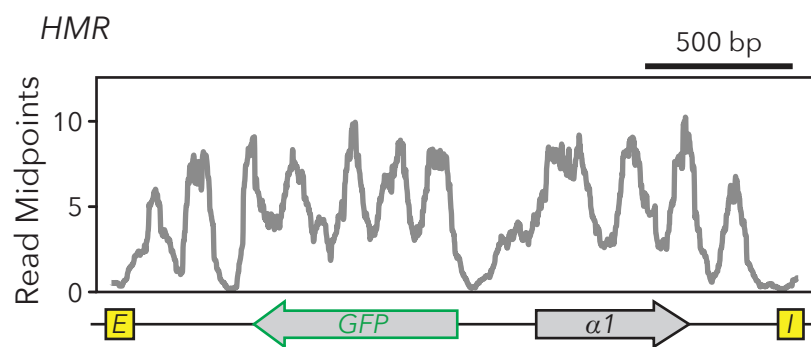


B



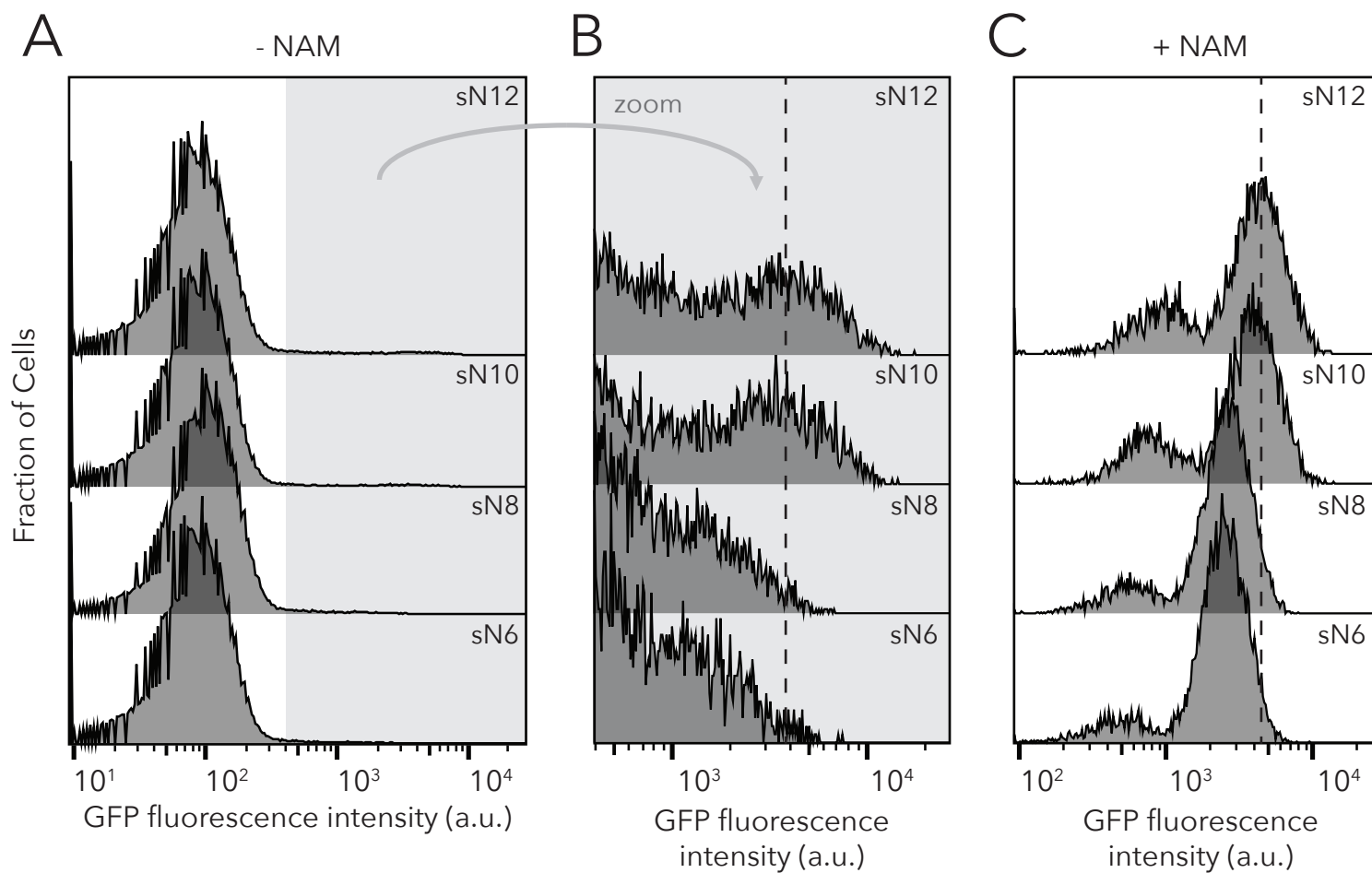
C

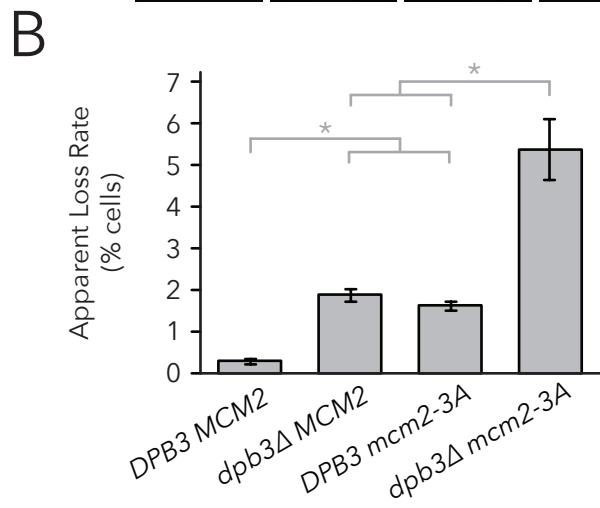
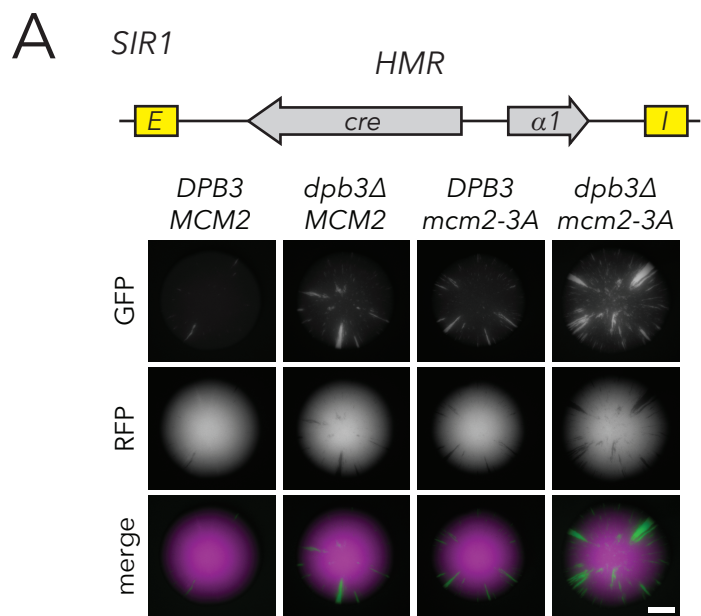




sir1 Δ

HMR

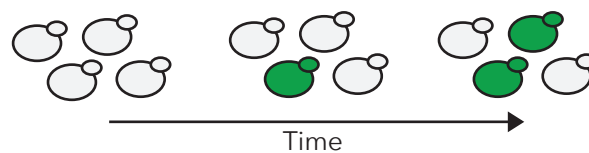




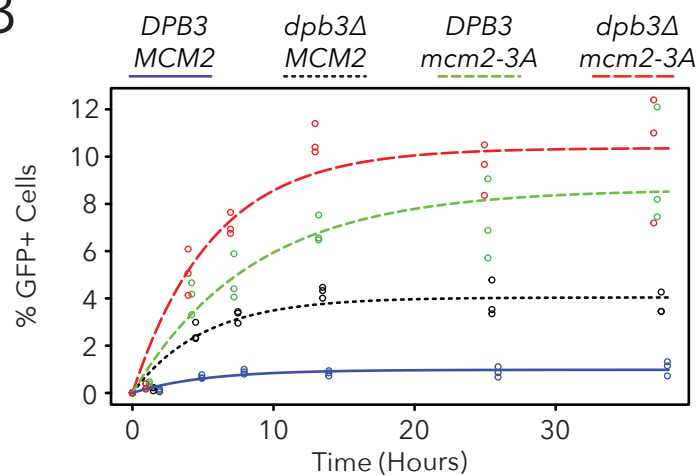
A

sir1 Δ 

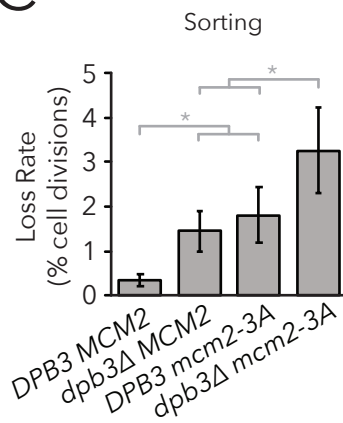
Sorted Cells



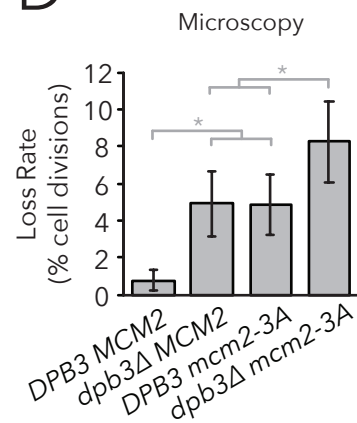
B



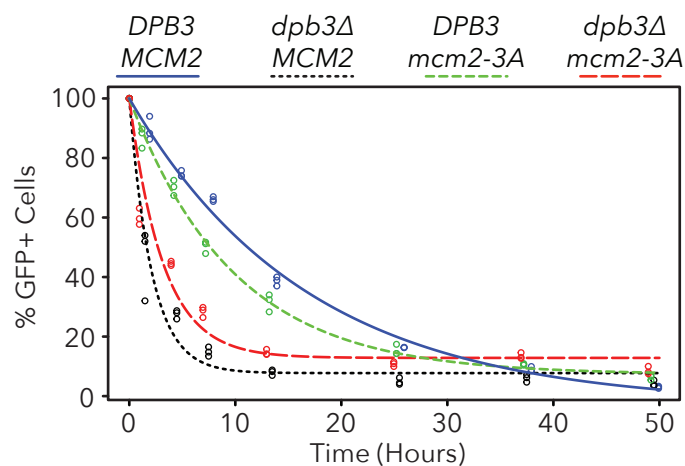
C



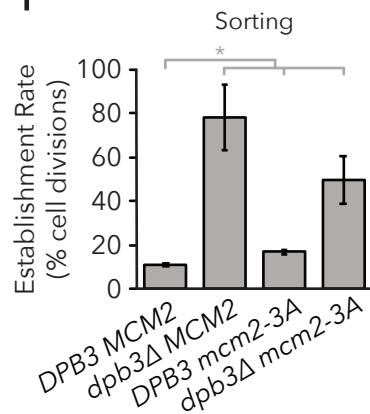
D



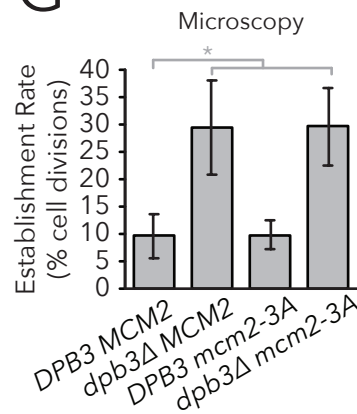
E



F

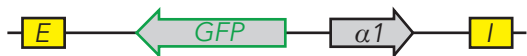


G

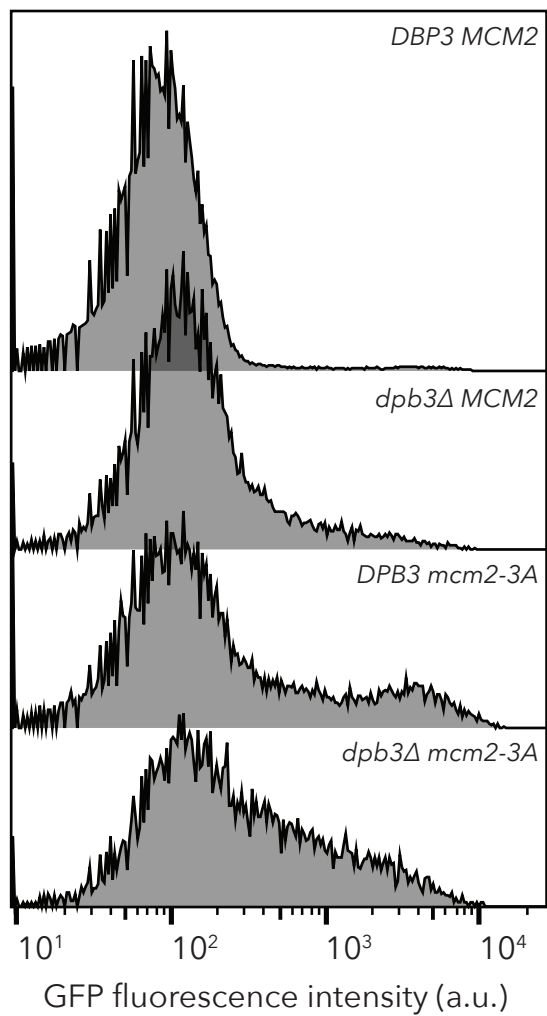


*sir1*Δ

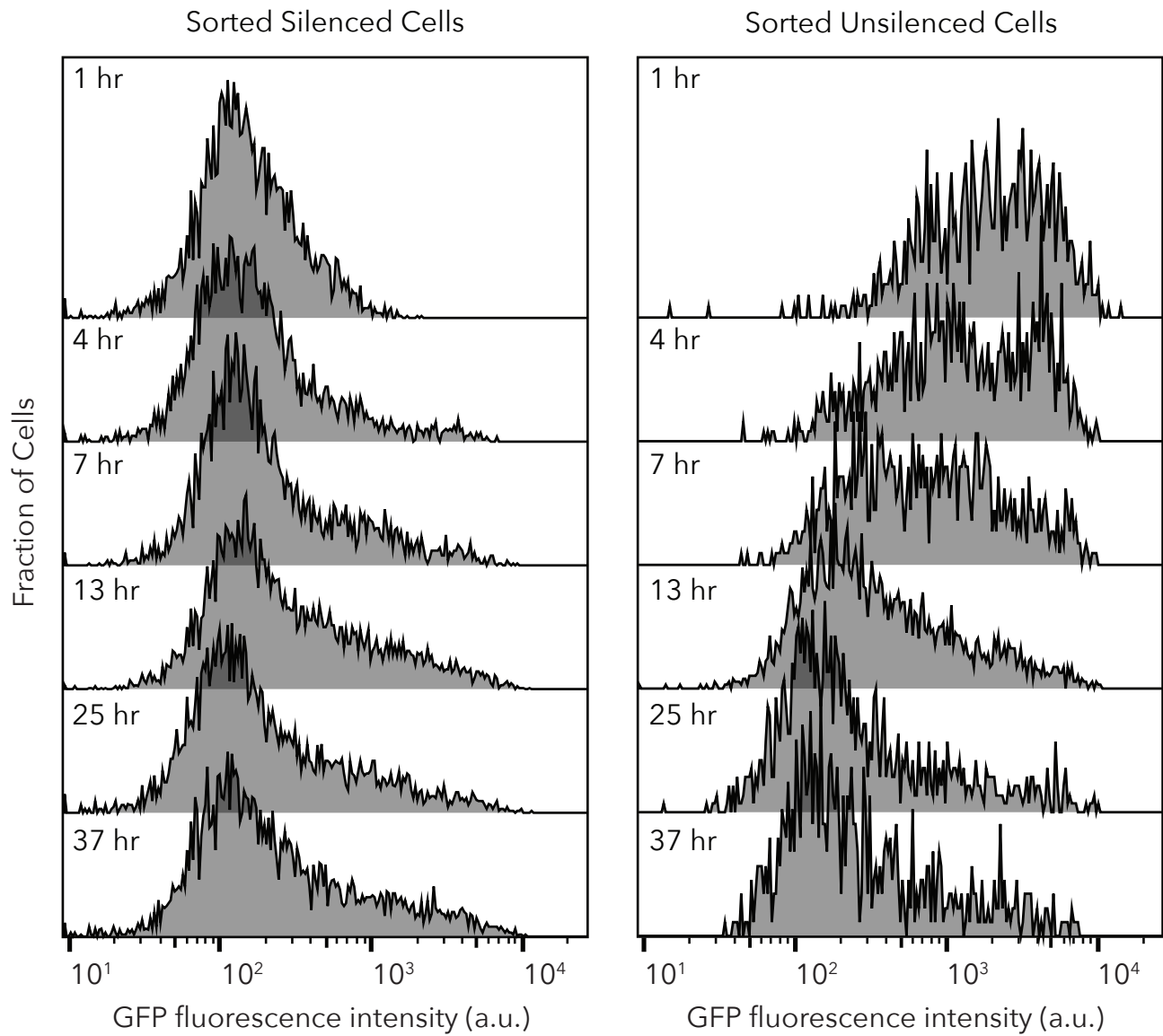
HMR

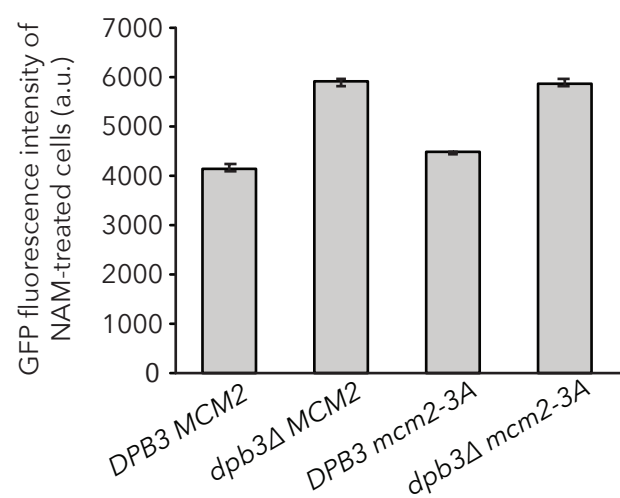


Fraction of Cells

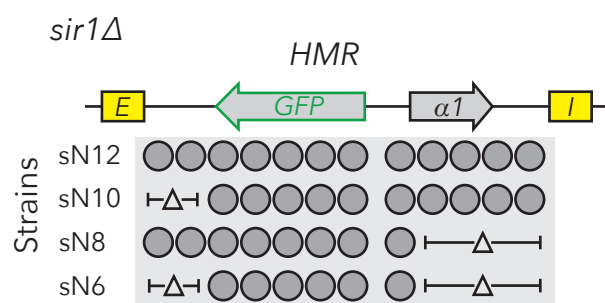


sir1Δ dpb3Δ mcm2-3A

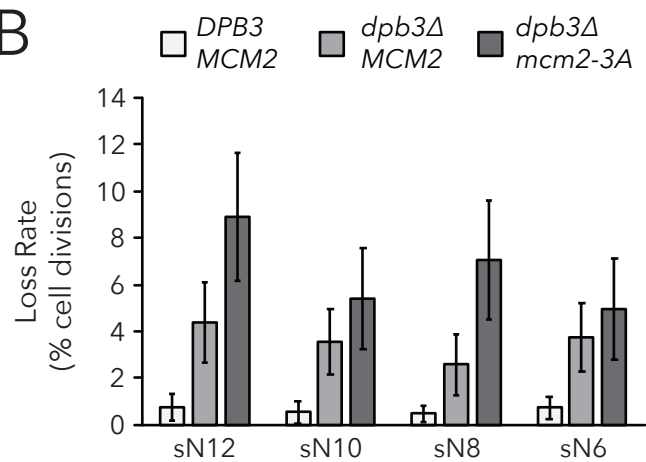




A



B



C

